4. Characteristics of Cellulose Acetates

4.1 Characterization and Physical Properties of Cellulose Acetates

Peter Zugenmaier

Institute of Physical Chemistry, Clausthal University of Technology, Arnold-Sommerfeld-Str. 4, D-38678 Clausthal-Zellerfeld, Germany
E-mail: Zugenmaier@pc.tu-clausthal.de

Summary: An overview is provided of the basic features of cellulose acetate of various degree of substitution in the solid and liquid crystalline state as well as in solution. These features represent a necessity for an understanding of the properties of these cellulose derivatives and further for mixed esters, which are not presented in this paper. Specifically, the crystal structure of cellulose triacetate will be addressed as well as structures in dilute and semi-dilute solutions. Thermal, viscoelastic and further properties in the solid state are discussed as well as flow behavior of solutions and their application in molecular weight determination, including false viscosity of commercial 2.5 cellulose acetates.

Keywords: structures of solids, liquid crystals, solutions; properties of fibers, films, thermoplastics; thermal, mechanical, viscoelastic properties; intrinsic viscosity; light scattering

4.1.1 Introduction

Cellulose acetate (CAc) represents a material with a wide range of behavior and application. It may be fully acetylated that is all three hydroxyl groups of the monomeric unit of the cellulose chain are derivatized or only two or one hydroxyl in a regioselectively or statistically manner. A material commercially widely used is the so-called 2.5 cellulose acetate (secondary CA), in which an average of 2.5 hydroxyl groups of a monomeric unit of the cellulose chains are acetylated. But this term is also applied, if the degree of substitution is somewhat lower or higher as well as the term triacetate (CTA) can be used for all cellulose acetates with a degree of substitution above 2.7.

The field of application for CTA and secondary CA (2.5 acetate) includes photographic film base, polarizing protecting film application in liquid crystalline displays to acetate staple fibers as air

 DOI: 10.1002/masy.200450407

and noise filters, cigarette filters, plastic materials for eyeglass frames, tool handles and toys to materials used in controlled release in agriculture, pharmaceutics, fragrances and polymer additives, in industrial coatings or as separation medium for membranes and stationary phase for entantiomeric separation etc. The advantage of cellulose acetate lies in low toxicity, low or almost non-flammability. It is produced from renewable resources and is biodegradable at least after pretreatment.

In the 1970th it was predicted by prominent scientists that progress in performance of polymeric materials would only be achieved through synthesis of new monomers leading to tailored polymeric materials with improved physical properties. But at the turn of the century, it became apparent that the progress and improvement of polymeric materials predominantly occurred by tailored processing and exploiting synergetic effects i.e. as mixtures, copolymers and composites comprising the advantages of the components involved. These improvements heavily rely on the characterization of the materials and on our understanding of fundamental processes as well as dynamics within the materials on one side and on the other side on the availability of methods of investigations, including the development of adequate equipment, which provides answers to our questions and provokes new ideas. Therefore, the physical properties of materials are closely interrelated with their characterization.

In this chapter we will evaluate the characterization and properties of cellulose acetate from a basic point of view in the solid state, in solution and liquid crystalline state. In the solid state we will address the crystal structure of CTA, thermal and mechanical properties of CAc as well as further physical properties, which are related to application. Most of the studies in the literature are performed on fibers, plastics or films. Experimental data for commercial secondary CA films with plasticizer are collected in Chapter 5.3 under standard conditions, additional data on yarn can be found in Chapter 5.1. Plastic materials are described in Chapter 5.5, membranes and chromatography in Chapter 5.6.

The molecular structure of cellulose acetate as molecular mass, chain stiffness, shape, interactions leading to aggregation and association, flow properties may be studied in solution and basic ideas derived that are important for applications. Solubility, adsorption of liquids and resistance of chemicals influence the usefulness of materials. We will discuss the solubility only for commercial cellulose acetates and leave the influence of special derivatization patterns of the

monomeric unit and along the chain to be introduced in Chapter 4.2 as well as the determination of these patterns by NMR. The lyotropic liquid crystalline state (lc) i.e. the structural changes of highly concentrated cellulosic solutions will be shortly described, since promising performances of filaments and yarn result by spinning of dope at high concentration from of this lc state with the advantage of reduced viscosity as compared to the isotropic solution.

We would like to mention numerous reviews and articles in encyclopedias and handbooks, in which important data for properties of cellulosics in conjunction with further materials are collected [1]. Cellulose acetate played an important role in the development of tools and methods for basic investigations of polymers. As this book commemorates a 100 years of cellulose acetate, we will begin with some historical remarks about the importance of cellulose triacetate for the acceptance of the macromolecular concept by Nobel Prize Winner Hermann Staudinger after a long lasting dispute with opponents who proposed aggregations of small molecules on one side and micellar structures of short chain on the other side to explain the behavior of biopolymers and synthetic polymers in solution and in the solid state.

4.1.2 Historical Remarks: Cellulose Triacetate as Macromolecule

The discovery and development of new experimental methods started a deeper insight into biological and synthetic materials at the beginning of the 20th century. The discovery of X-rays and their useful application in structural research in the field of solid state matter as well as the development of IR-spectroscopy for dynamical studies and the development of the ultracentrifuge, the electrophoresis and improvement of the osmotic cells for investigations in solutions gave rise to the developments of the macromolecular concept and introduced chain molecules.

Staudinger [2] himself regarded the year 1921 as turning point in the field of cellulose chemistry, since in this year Karrer [3] published a new concept about the constitution of starch and cellulose, which led to a decade of controversial discussions. Karrer proposed that starch and cellulose consist of anhydrides of maltose or cellobiose, respectively, as result of his degradation experiments. The colloidal solutions formed exist of aggregates of secondary bonded small molecules, so called micelles in his view. This idea was supported by the small unit cell of cellulose determined by X-ray diffraction and the molecular weight determination by Hess [4] and

Bergmann [5] on cellulose acetates and cellulose ethers by the cryoscoptic method. A large depression of the freezing point led Hess to the conclusion that this observation is caused by glucose anhydride. Years later it was found that this method cannot be applied to cellulose acetate and that the osmotic pressure method actually led to high molecular weights. Biologists supported Karrer's opinion, since they confirmed the ideas of K. v. Naegeli who found in the 1860th that cotton and other high molecular biopolymers crystallize, and he concluded that the crystalline domains, which he called micelles, cause the colloidal character in solutions. In 1925 Herzog [6] observed that the crystallite size of cellulose in the solid by the X-ray method agreed with the size of the micelles of nitro cellulose in solution determined by diffusion. These findings were corrected by the author [7] several years later (1933).

The idea that cellulose is a low molecular weight compound was generally accepted in the years 1921 to 1927, since the arguments by Karrer, Hess and Bergmann could not easily be contradicted in the field of cellulosics.

In 1920 Staudinger [8] already stated for polymers that a numerous number of small basic molecules are linked together to form macromolecules, and he was able to confirm the high molecular weight by end group analysis in the case of polyoxymethylene [9] and considered this compound as a model for cellulose (1925). Some of the supporting arguments for aggregation of small molecules lost their validity, when found that a small unit cell for crystalline cellulose as established by X-ray diffraction does not contradict the presence of long chain molecules [10] (1927).

Sponsler and Dore [11] (1926) published a model of cellulose as a chain molecule derived from X-ray experiments based on atomic distances of organic compounds with linked pyranose rings and explained the 10.25 Å fiber repeat by primary valances between the β-linked anhydroglucopyranose units (AGU). The mistake of alternating 1-1, 4-4 linkage of the AGU was corrected by Haworth [12] and others. This corrected formula represents the base for structural considerations by Meyer and Mark [13] and others since 1928. The chain structure of cellulose was further supported by hydrolytic scission leading to oligosaccharides (Zechmeister [14]) and the β-linkage was further supported by Freudenberg [15]. The length of the chain was not determined in these investigations. Meyer and Mark proposed a model for this problem, especially for colloidal solutions. Taking the proposal of Herzog that the solid state micelles resemble those in solutions

as well as the result of Sponsler and Dore, they proposed that the primary valence chains of definite length form blocks or micelles and are bound together by strong cohesion forces so called micellar forces. They will not be separated in solution as occurring for small molecules [16]. The micelle was regarded as the basic unit describing high molecular weight compounds (cf. Fig. 1). It was assumed by X-ray investigations (line width) that 30 to 50 AGU [13] later 60 to 100 AGU [17] form the primary valence chain (the projection of one AGU on the chain axis is about 5 Å) and about 40 to 60 chains built a single irreversible micelle. The molecular weights of the "macromolecules" determined by osmotic pressure experiments were termed micellar weights. The high viscosity of cellulose and their derivatives in solution and also the swelling seemed to be explained by the micellar model with long chains. This idea was well accepted by colloidal chemists and biologists but was proofed to be wrong by measurements of the molecular weights of cellulose triacetate, which were obtained by polymer analogous reaction. Meyer and Mark later abandoned the micellar model and turned to the macromolecular concept.

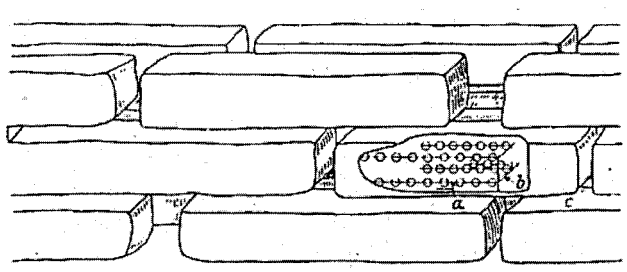

Fig. 1. Model of the morphological built-up of a Ramie fiber according to Meyer and Mark (from [2]).

The idea of Staudinger that the entities or basic units in solution are dissolved macromolecules and not micelles proved to be correct, and he was awarded the Nobel Prize in Chemistry 1953 "for his discoveries in the field of macromolecular chemistry". He was able to prove his early assumptions with methods of organic chemistry and set the foundation of concepts in this field that are still recognized today. He introduced what he called the polymer analogous derivatization of cellulose, i.e., he derivatized cellulose without changing the degree of polymerization DP and measured the same DP (actually the corresponding molecular weight) starting from cellulose to cellulose triacetate and back to cellulose or to cellites (not fully substituted cellulose acetate),

methyl cellulose and methylacetyl cellulose. The DP was determined by osmotic pressure experiments and later quite often by viscosity applying the intrinsic viscosity [η] relationship:

$$[\eta] = \lim_{c \to 0} \eta_{sp}/c = K_m M^a \qquad (1)$$

c concentration, η_{sp} specific viscosity, K_m experimental determined constant for a specific solution adjusted sometimes from low molecular weights to higher molecular weights, M molecular weight and the value for **a** depending on shape and solution properties of the molecules. Staudinger assumed **a** = 1 for cellulosics as rod like macromolecules in solution [18] even in his later years (cf. Nobel lecture 1953) and argued that the cellulose molecules are present as rods in the solid fiber and in the same form in solution as most extended chains. This value **a** = 1 is correct for cellulose trinitrate for not too high DP (DP<1000). For cellulose acetates a value of **a** = 0.9 was proposed by careful evaluation of experiments in 1951 [19] after a long discussion of various experimental results but not accepted by Staudinger. Tables 1 and 2 list the results of Staudinger's original investigations [2].

Table 1. Degree of polymerization (DP) of cellulose triacetate (CTA) in comparison to the original cellulose and the deacetylated one by polymer analogous reaction (from [2]).

Cellulose	CTA	cellulose (deacetylated CTA)
500	505	490
790	795	780
1000	970	955
1570	1670	1680

Table 2. DP of polymer analogous cellulose triacetate, cellite, methyl- and methylacetyl cellulose (from [2]).

Triacetate	cellite	methyl cellulose	methylacetyl cellulose
165	165	160	185
185	185	170	210
205	205	210	195
390	390	410	425

Staudinger's main idea was a molecularly dispersed distribution of macromolecules in dilute solution. However, he considered aggregation for higher concentrations. From nowadays point of view, it turns out that polymer aggregation in dilute solution is neither as general as assumed by Meyer and Mark nor generally absent as claimed by Staudinger. The breakthrough of the macromolecular concept was achieved by the systematic study of the chemical and physical properties of a homologous series from oligomers to high polymers of polyoxymethylene resulting that all these materials rest on the same structural principal as well as by polymer analogous substitution of cellulose to obtain cellulose triacetate (Table 1) or nitrate and the continuation of polymer analogous reactions to further derivatives (Table 2) and back to cellulose obtaining the same degree of polymerization.

4.1.3 Structural Characterization of Crystalline Cellulose Acetate

The maximal degree of acetylation of cellulose occurs in cellulose triacetate CTA with 62.5% acetic acid or 44.8% acetyl content. Characteristic for CTA is its solubility in chloroform, and CTA is not soluble under normal conditions in acetone. Therefore, CTA is referred to "chloroform soluble acetate" or since CTA is derived as a primary product as "primary acetate". Besides the fully substituted triacetate all acetates, which are soluble in chloroform, will be addressed as "primary acetate". The most important acetate for application represents acetate with an acetic acid content between the triacetate and diacetate that can be characterized by the solubility in acetone. These materials are obtained by partial deacetylation of triacetate and are called secondary acetate (CA) or "acetone soluble acetate". In older publications this secondary acetate with an acetic acid content of 50-58% produced by Bayer is called "Zellit". The amount of acetyl groups for cellulose acetate is provided by different terms in various publications, e.g. the degree of substitution DS or the acetyl group content or the acetyl acid content in % as increase of the molar mass of an anhydroglucopyranose unit (AGU). The conversion is represented for the most often discussed cellulose acetates in Table 3.

Properties of the acetates may also depend on the average distribution of the acetyl groups at the three possible sites of the anhydroglucopyranose unit (AGU) and on the distribution along the chains. These distributions may result in differences of the index of crystallinity, if crystallization occurs and in various solution properties and have led to contradictory results as will be pointed out later. The results collected in Table 4 may serve as an example of various distributions at the

different sites of the AGU.

Table 3. Conversion of degree of substitution DS of cellulose acetate CAc in acetyl and acetic acid content.

Compound	DS	acetyl content	acetic acid content
monoacetate	1	21.1%	29.4%
diacetate	2	34.9%	48.8%
2.5 acetate	2.5	40.1%	56.2%
triacetate	3	44.8%	62.5%

Table 4. Distribution of acetyl groups by homogenous deacetylation of CTA in different media for various reaction times at 80 °C (from [20]).

Media	mol/mol of AGU	t / h	DS_{Ac} [a]	DS_{Ac} NMR	pattern of substitution C2	C3	C6
HMDA	2.3	2.5	2.6	2.65	0.8	0.85	1.0
$(NH_2\text{-}(CH_2)_6\text{-}NH_2)$		4.5	2.41	2.4	0.65	0.75	1.0
		9	1.87	1.95	0.45	0.55	0.9
		14	1.33	1.5	0.2	0.45	0.85
		24	0.75	0.75	0.05	0.1	0.6
DMA	4.5	5	2.55	2.55	0.75	0.8	1.0
$(HN(CH_3)_2)$		11	2.06	2.0	0.5	0.5	1.0
		15	1.84	1.8	0.35	0.5	1.0
		20	1.59	1.6	0.3	0.4	0.9
		24	1.45	1.2	0.2	0.3	0.7

[a] Functional group analysis

4.1.3.1 Solid State Characterization by Fingerprint Methods

The characterization of solids can be achieved at various levels. The simplest attempt may be a fingerprint procedure by spectroscopic means, e.g. IR (cf. Appendix A1) or NMR, as well as by diffraction, e.g. X-ray or electron scattering. The highest level of characterization may include a complete structure determination providing coordinates of every atom in the crystalline structure. Also, the crystallite size, disorder and motion of the atoms may be of interest in an evaluation of mechanical properties.

Generally, two kinds of X-ray diffractograms are available for crystalline polymers. The Debye-Scherrer pattern from samples with isotropic distributed crystallites and the fiber patterns where the crystallites are uniaxially oriented in native fibers or in stretched or drawn samples. A schematic representation of a geometric model of arrangements and the resulting X-ray diagrams

are depicted in Fig. 2. The positions of the reflections are governed by the unit cell size and by space group symmetry elements. The intensity of the reflections is caused by the interference of radiation that is by the scattering from atoms at individual positions. Therefore, the overall appearance of a diffractogram (Debye-Scherrer or fiber pattern) differentiates between various crystalline structures.

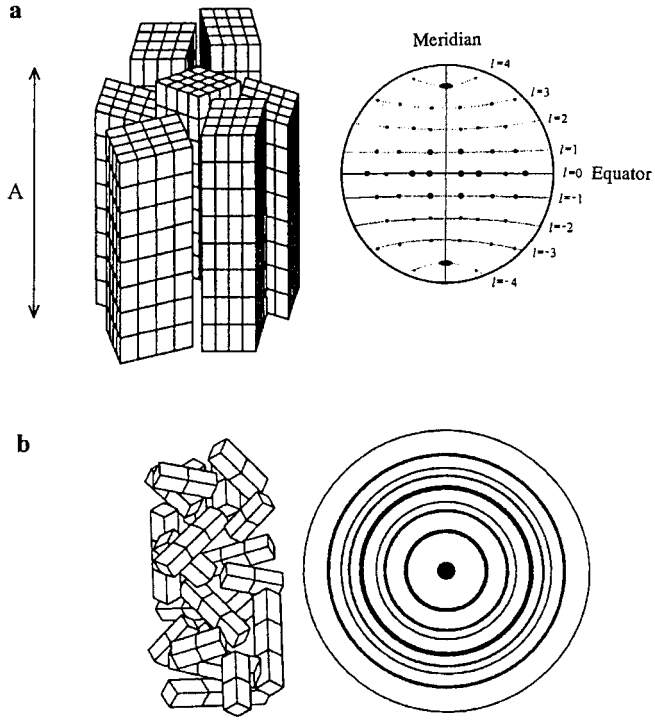

Fig. 2. Schematic representation of the distribution of crystallites and the resulting X-ray diagrams. (a) Uniaxially distributed crystallites around A leading to a fiber pattern. (b) Isotropic arranged crystallites producing a Debye-Scherrer pattern of concentric rings (from [21]).

A complete structure determination requires an elaborate procedure for polymers that includes additional information by conformational and packing analysis, by spectroscopy or other specific information from model compounds as e.g. bond lengths and angles or chain arrangements, parallel or antiparallel packing for chiral molecules, which might be available from low molecular

mass compounds.

4.1.3.2 Polymorphism of Cellulose Triacetate CTA

For CTA, Hess and Trogus established two kinds of crystalline structures called polymorphs by X-ray diffraction that produce different Debye-Scherrer diagrams or fiber patterns. They called these structures CTA I and CTA II [22, 23]. CTA I was obtained by heterogeneous acetylation of native cellulose I, CTA II by reacting regenerated or mercerized cellulose II as starting materials. Both polymorphs led by saponification back to their original materials, which were confirmed by Sprague et al. [24]. For high quality diffractograms the CTAs were heat treated in the 210 to 280 °C range for a few minutes.

The fibrous transformation of CTA I to CTA II was achieved by superheated steam treatment without any dissolving process [25] but CTA II could not be converted back to CTA I. Nevertheless, it was reported that CTA I was obtained by special treatment from mercerized cellulose II [26] that is a conflicting observation from a structural point of view and will be discussed later.

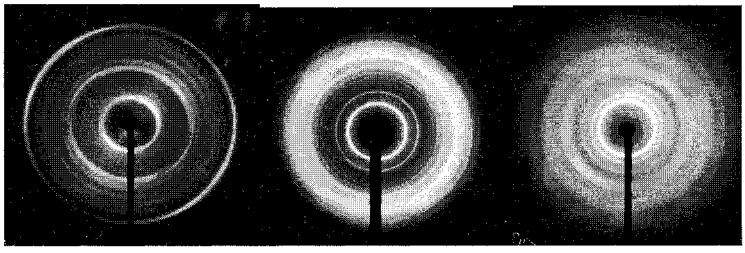

A B C

Fig. 3. Debye-Scherrer patterns of CTA I (A), CTA-N (B), and CTA II (C).

In addition, a third pattern, CTA-N, was observed with nitromethane build into the crystal lattice. The fact that solvent was included in the crystal domains was first established by the Freiburg group in the laboratory of Husemann [27], although the polymeric single crystals of quadric shape crystallized out of mixed n-butanol/ nitromethane solutions were earlier outlined in a publication by Manley [28]. The loss of the solvent by taking the X-ray exposures led to CTA II and made to propose CTA II single crystals [28]. The three different Debye-Scherrer patterns of CTA are

presented in Fig. 3. Each of the CAc pattern can be used to identify the kind of structure present. The same information is contained in diffractograms of Fig. 4 taken by an electronic detector that are easier to evaluate than photographs and for reasons of comparison, the X-ray patterns of oligomeric peracetylated crystals are added to demonstrate that these crystal structures are close to the one of CTA I. In Fig. 5 the ^{13}C CPMAS spectra of CTA I and II as well as the corresponding oligomers are shown and provide further information. A split of NMR signals of all ring carbons except of C1 occurs for CTA II, which means that at least two conformational different AGU (residues) are present in the crystals [29, 30]. Only one peak as for CTA I suggests a single conformation of the AGU and can explain the crystal structure of CTA I. These spectra provide useful information in discussing the molecular and crystal structures of CTA I and II and some valuable information can be drawn from the structures of the oligomers.

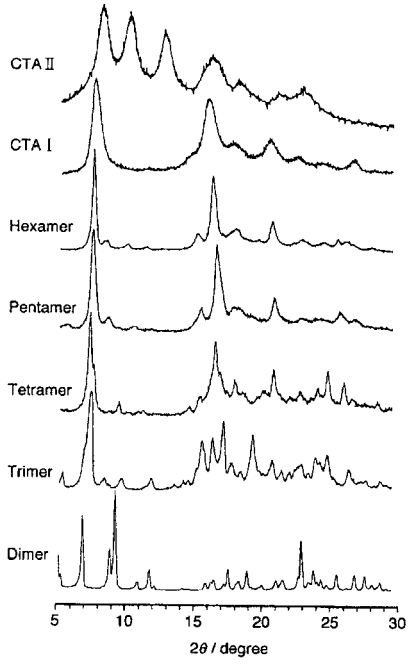

Fig. 4. X-ray diffractograms of CTA I, CTA II and oligomeric CTA (DP=2-6) (from [29]).

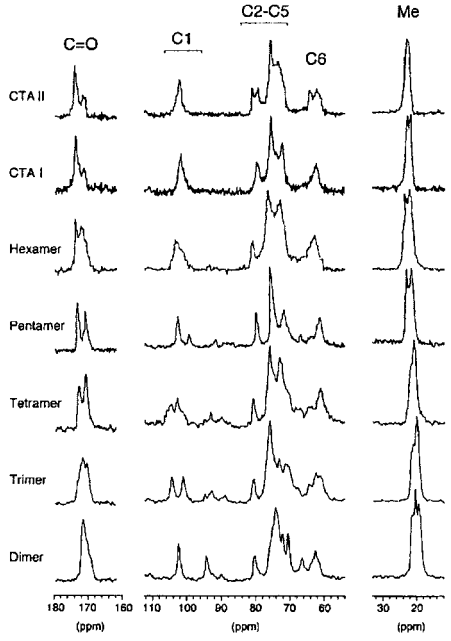

Fig. 5. ^{13}C CPMAS spectra of CTA I, CTA II and oligomeric CTA (DP=2-6). Peak intensities of the methyl region are shown at 40% reduction (from [29]).

The transformation from CTA I to CTA II can also be achieved by exploiting the solvent complexed state CTA-N [31]. This procedure provides additional information on the structural transformation process of these polymorphs. The fiber pattern of CTA representing CTA I in Fig. 6A has been obtained by heterogeneous acetylation of Ramie fibers. This fiber was then placed over nitromethane vapor resulting in the CTA-N structure (Fig. 6B), and when this CTA-N fiber was annealed at high temperature, the solvent is lost and the fiber transforms to CTA II (Fig. 6C). As expected the transformation of native Ramie cellulose I to CTA I is reversible as is the one from CTA II to cellulose II. Also the uptake of nitromethane from CTA II and the loss of nitromethane from CTA-N take place reversibly that means the loss of nitromethane from CTA-N always leads to CTA II. Only the step from CTA I to CTA-N was found to be irreversible. All possible transformation of crystalline CTA are collected in Fig. 7 that also implies a proposed deacetylation of CTA I, obtained by spinning of a lyotropic liquid crystalline dope of CTA II, to cellulose IV, which represents a further polymorph of cellulose quite similar to cellulose I.

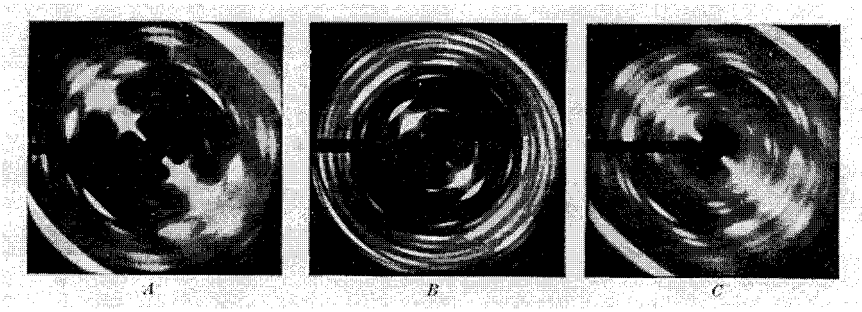

Fig. 6. Fiber patterns with fiber axis diagonal of CTA I (A), CTA-N (B) and CTA II (C) from a Ramie fiber heterogeneously acetylated (A), placed over nitromethane vapor (B), and successive annealing (C) (from [31]).

Recently, it has been confirmed that the chain molecules of native cellulose I are arranged in parallel fashion, those of cellulose II in an antiparallel fashion as schematically represented in Fig. 8. From this point of view a chain reversal from parallel to antiparallel arrangement takes place during the conversion from CTA I to CTA II, since CTA I can be converted to cellulose I and CTA II to cellulose II (cf. Fig. 7). As will be discussed later, CTA I also has been proposed as

parallel arranged structure, and CTA II is packed in antiparallel fashion. This change of direction of the chains takes place in an oriented fiber with no change in degree of orientation but with a change of lateral crystallite dimension expressed by the width of the reflections on the equator and layer lines (cf. Fig. 6). The smallest width of reflections observed for the CTA-N structure corresponds to the largest crystallite size according to the Scherrer equation. A theoretical model to explain these observations has been developed by assuming interdiffusion of parallel up running fibrils into parallel running down fibrils. The driving force is the interaction enthalpy of variously positioned chains. The crystallite size depends on the strength of the interaction between up and down running chains [33].

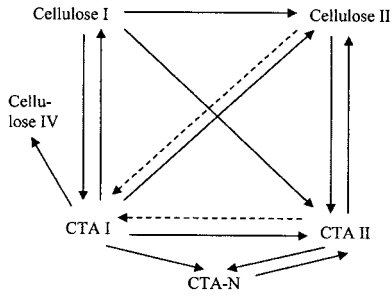

Fig. 7. Possible conversions of different polymorphs of cellulose and cellulose triacetate (CTA). The dotted lines represent recent findings [32].

The CPMAS ^{13}C NMR (cross polarization and magic angle spinning carbon-13 nuclear magnetic resonance) and X-ray studies of cello-oligosaccharide acetates [29] point to the fact, that the spectra as well as the X-ray diagrams are well comparable with CTA I and not with CTA II (cf. Figs. 4, 5). Specifically, the chemical shifts of the hexamer and pentamer agree with those of CTA I. The chain arrangement of the crystal structure of the peracetylated trimer and the proposed space group of the tetramer favor parallel packing in contrast to the cellulose oligomers that are packed in antiparallel fashion. These observations are strong hints for a parallel chain packing in solid CTA I.

The X-ray pattern depicted in Fig. 9A has been obtained from a liquid crystalline, low molecular weight CTA dope and represents CTA I. In contrast high molecular weight CTA always shows X-

ray patterns of CTA I with traces of CTA II. In this experiment an unusual parallel chain arrangement in the crystalline state was formed out of solution, which normally leads to CTA II [34]. However, saponification of this CTA I structure resulted in a mixture of cellulose II and IV.

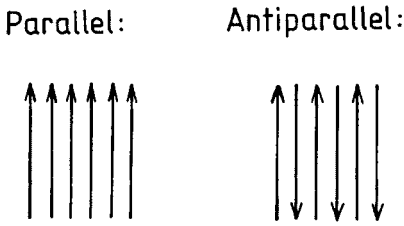

Fig. 8. Schematic representation of parallel and antiparallel running chains for chiral molecules having a directional sense.

It has to be noted that all the well-developed X-rays patterns of CTA I have been obtained by annealing the originally oriented fibers at relatively high temperatures (ca. 250 °C for 15 min for CTA I and II). The original CTA fiber as taken from the heterogeneous reaction leads to a pattern represented in Fig. 9B, which shows reflections between the first two strong equatorial reflections of CTA I of Fig. 9A. This modification has not been included in the discussion of the structure of CTA nor have these reflections been considered in the evaluation of the size of the unit cell. This diagram may represent another polymorph or may lead to a different unit cell for CTA I as currently proposed. This non-annealed modification is regarded as the active stationary phase in elution chromatography in chiral separation of enantiomers [32].

4.1.3.3 Crystal and Molecular Structures

Fiber patterns as those depicted in Fig. 6 contain the information to serve for an evaluation of the molecular and crystal structure. The layer line spacing in connection with the appearance or missing meridional reflections lead to the determination of the fiber repeat c and the kind of symmetry (helix) present in the fiber. For CTA I and CTA II a second order meridional reflection mirrors a 2_1 screw axis along the c-axis and for CTA-N an eighth order meridional reflection suggests an eight fold helix or a fourfold helix with a cellobiose acetate as motif. Generally, all parameters establishing the unit cell are available from X-ray data, and these parameters represent a prerequisite for a crystal structure determination. The space group can be proposed with the

detected symmetry elements (cf. Table 5) but often the solution is ambiguous. Extremely helpful are electron diffractions on polymeric single crystals, which actually are too small for performing a single crystal structure determination as commonly applied on low molecular mass compounds. The unit cell proposed for CTA II was confirmed by electron diffractions and seems quite reliable while difficulties for the unit cell determination of CTA I are not yet resolved completely, since some disturbing reflections as discussed cannot precisely be assigned. In case of CTA I no electron diffraction patterns are available.

A conformational analysis on the basis of computer modeling may first provide possible conformations of CTA that are constraint to the fiber repeat of about 10.43 Å for CTA I, 10.54 Å for CTA II and 41.36 Å for CTA-N. All these conformations have a rise per residue of ca. 5 Å in common, which also holds for three fold helices established for other cellulose derivatives.

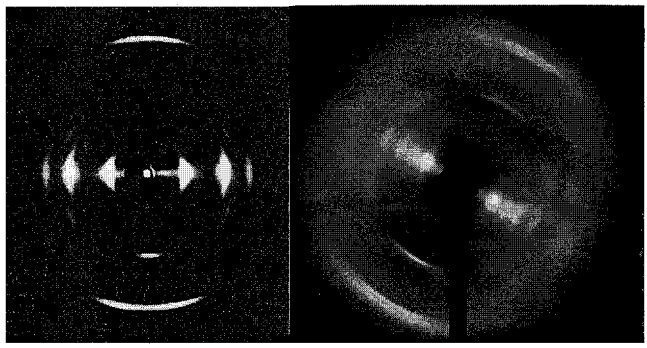

A B

Fig. 9. Fiber X-ray diagrams: A for CTA (DP=300) produced from liquid crystalline dope (trifluoroacetic acid/ H_2O, 100:8 w/w) by film casting and hand-pulled (note the close similarity with CTA I polymorph) (from [34]); B for CTA I (from original Ramie fiber) as obtained from the derivatization reaction without annealing (fiber axis diagonal in this photo).

Proceeding with a packing analysis on the basis of minimizing potential energies and inclusion of the X-ray intensities (structure factors) of the reflections, after the necessary corrections have been applied, a molecular and crystal structure model will be obtained. These models strongly depend on the assumed unit cell and potential energy parameters. Therefore, it is a necessity to confirm these structures by additional experimental data as derived for model compounds of oligomers and by other means as spectroscopy.

CTA I was proposed by applying the described procedure as parallel chain arrangements with a 2_1 screw axis along the chain axis [35]. This proposal is depicted in Fig. 10 in two projections. Since the two independent chains of the unit cell are identical in conformation and placed on an almost exact translational symmetry position, the base plane of the unit cell presented in Table 5 may be cut in half and a one-chain monoclinic space group $P2_1$ proposed with the only CTA chain placed on the 2_1 screw axis. This proposal will also fulfill the single AGU requirement as basic unit of the crystalline structure being deduced by the NMR results [29, 30].

Table 5. Unit cells of various polymorphs of CTA. Axes in Å and angles in degrees, densities ρ in g cm^{-3}.

Materials	a	b	c	α	β	γ	ρ	space group	ref.
CTA I	23.63	6.27	10.43	90	90	90	1.24	$P2_1$	[35]
CTA I §	11.82	6.27	10.43	90	90	~90	1.24	$P2_1$	
CTA I *	11.27	6.00	10.47	90	90	86.15	1.34	$P2_1$	[36]
CTA I &	24.31	5.15	10.53	90.1	90.0	83.9	1.46	$P2_1$	[32]
CTA II	24.68	11.52	10.54	90	90	90	1.29	$P2_12_12_1$	[37,38]
CTA-N#	21.15	21.15	41.36	90	90	90	1.01	not known	[27]

§ Omitting the broad (300) reflection
* Small, one-chain unit cell; Wada et al. [39] proposed the same unit cell with $\gamma > 90°$ only
# Alternative a = b = 15.4 Å . One nitromethane molecule per AGU
& Computer modeling only

Two other monoclinic one-chain unit cells were proposed and listed in Table 5 [32, 36]. However, these unit cells have a higher density as compared to the more stable CTA II and may be rejected on this property. The model of Wolf et al. [32] was derived on pure molecular modeling calculations with the assumption of parallel chain arrangements in a two-chain unit cell. The crystal structure, space group $P2_1$, resemble the one of Stipanovic and Sarko but with a definite monoclinic angle γ and with extremely high density. An also tested possible antiparallel arrangement exhibits higher potential energy, an orthorhombic lattice and almost the same too high density of 1.42 g/cm^3. These results point towards a larger unit cell that does not necessarily contradict the X-ray and NMR diagrams of Figs. 4 and 5. The X-ray pattern of CTA I exhibits a reflection as a shoulder ahead of the second strong reflection that is more pronounced in the similar pattern of the hexamer. The proposed small one-chain unit cells cannot explain this reflection. Concerning the NMR spectrum, a single monomeric AGU may not contradict a larger

unit cell and is suggested by the pattern of the hexamer, in which the monomeric units certainly are not related by symmetry operations but nevertheless exhibit a comparable spectrum as CTA I with six independent AGUs.

The X-ray diagram of CTA I resembles actually the pattern of trimethyl cellulose (TMC), for which an orthogonal unit cell was established by electron diffraction with a = 4.64 Å, b=43.2 Å and c= 10.42 Å [40]. But the space group and structure have not yet been determined. Another unit cell has been also proposed by the evaluation of high precision Debye-Scherrer imaging plate data [41].

At the present the proposed structure of CTA I [35] can at least be regarded as a good approximation until a definite structure is established. Further, the a-axis can be cut in half without any loss, if the broad reflection (300) is omitted, of which the origin is questionable. The intensities of the reflections with this smaller unit cell agree with the experimental values, which suggest that the relative mean positions of the molecules in space are correct, and the density of the unit cell seems reasonable. The space group may be proposed as $P2_1$, the molecular axis coincides with the 2_1 screw of the space group symmetry, and the NMR data with one single AGU agrees with this proposal.

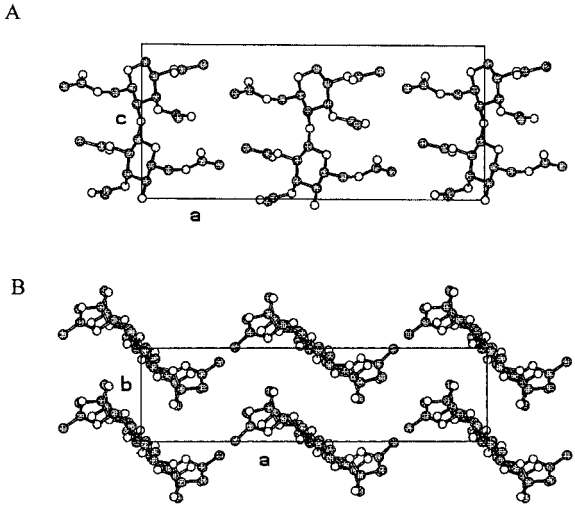

Fig. 10. Representation of the structural model of CTA I in two projections: A: perpendicular to the a, c-plane; B: down the helix axis (c axis) (omitting the hydrogen atoms).

The crystal and molecular structure of cellulose triacetate II (CTA II) [38] was derived from X-ray and electron diffraction analysis as well as modeling techniques using the central fixed residue of cellotriose undecaacetate [42]. The chain conformation has been assumed to possess a 2_1 screw axis as suggested by the single crystal structure of the peracetylated trimer, and the chains pack in pairs in an antiparallel fashion forming an orthorhombic unit cell (Table 5), space group $P2_12_12_1$. An X-ray fiber pattern for CTA II is depicted in Fig. 6C and a polymeric single crystal, the electron diffraction pattern thereof as well as the projection of the chains on the a, b-plane in Fig. 11. Dorset [43] used the available structure factors and constructed a potential map that is shown in Fig. 12 providing an excellent picture of the placements of the CTA chains. A projection of chains on the b, c-plane is provided in Fig. 13A.

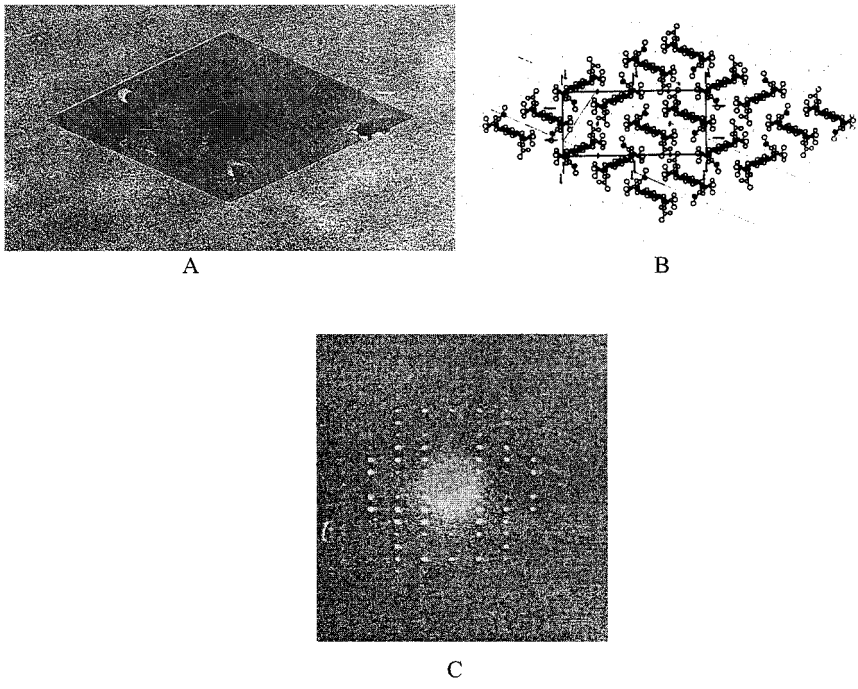

Fig. 11. Shape of a polymeric single crystal of CTA II viewed through an electron microscope (A) and placement of the CTA chains on the basic crystallographic a, b-plane (B), and the observed electron diffraction of the single crystal representing the a, b-plane (C) (from [38]).

However, if the intensity distribution of the fiber X-ray diagram is calculated and compared with the experimental one, some disagreement can be found (Fig. 14). Certainly, more knowledge about the structure of cellulosic chains is gathered today, especially that more than one stable residue conformation has been found and the molecular modeling by computer calculations has considerably improved. According to NMR studies, two different AGUs have been detected and can easily been taken into consideration, if the actual 2_1 screw symmetry elements between the chains are seriously accepted that means a dimer has to be considered as the basic building unit for the chains.

CTA-N exhibits an unusual long fiber repeat (cf. Table 5) and a meridional reflection on the eighth layer that suggests an eightfold helix with the common ca. 5 Å repeat per residue. An excellent solution for the conformation has been found with a left-handed 8/5 helix and is represented in Fig. 13B. This conformation contrasts the sheet like structure of CTA I and CTA II with a cylindrical shape, and it also points towards a change of backbone conformation that might occur for CTA interacting with solvent in solutions.

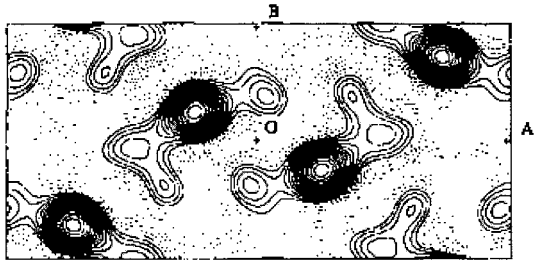

Fig. 12. Electron density in the basic a, b-plane of CTA II by evaluation of the diffraction pattern. Note the placements of the chains are clearly expressed (from [43]).

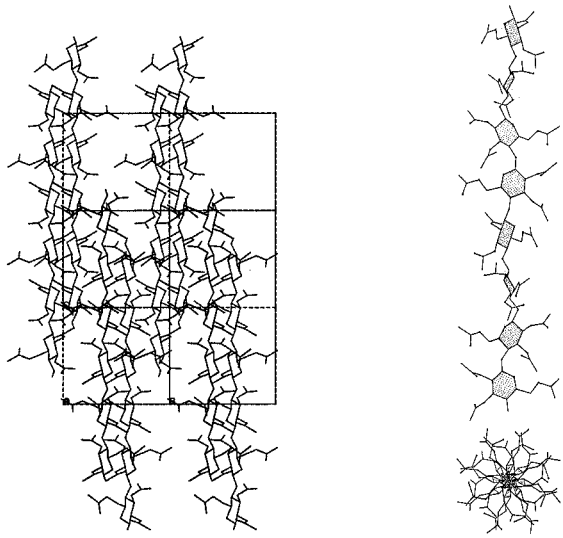

Fig. 13. A: Representation of the projection of the molecules on the b, c-plane of CTA II (from [41]) and B: CTA-N conformation in two projections along the chain axis and down this axis.

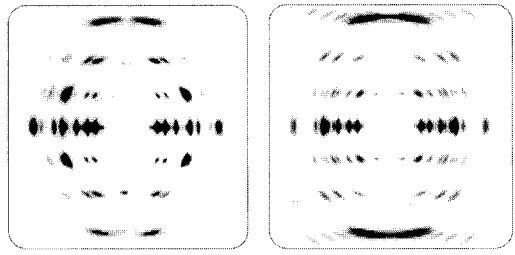

Fig. 14. Comparison of an experimental (left picture) and calculated (right picture) X-ray diagram of CTA II (from [41]).

Cellulose acetate with DS = 2.5 or 1.75 derived by deacetylation of CTA also exhibits partially crystalline structures. The evaluation of the powder X-ray pattern suggests the modification of CTA II [44], which leads to the assumption that several trisubsituted anhydroglucopyranose units are succeeding each other. The segmental length was determined to 19 units on the average for CA (DS ~2.5) [45] that implies a blocky structure for this cellulose derivative and fills into the

picture of secondary CA in solution to be addressed later.

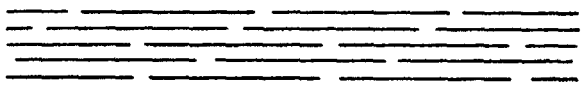

Fig. 15. Idealized representation of a structural model for low molecular weight CTA and secondary CA. Crystalline and non-crystalline sections are adjacent along a chain. The crystalline domains are only a few molecules wide.

An idealized model for fibrils or crystalline domains of all kind of cellulose acetates is represented in Fig. 15 for low molecular weight compounds as present in commercial products with a normal DP range of 150 - 360 for CTA and 100 – 200 for secondary CA. Crystalline and non-crystalline blocks are arranged containing antiparallel chains along the fibril. Chain ends will enhance the disorder but may not be separated to form a section of its own.

The density of the crystalline triacetate is smaller than the non-crystalline section as required by investigations of Malm et al. [46] and may include water molecules. Actually the picture in Fig. 15 is a stretched topological form of the model for irreversible aggregates of secondary CA in acetone solutions proposed by Burchard as shown in Fig. 49. For long chain molecules the established fringed micelles may describe the topology of the fibrils with successive crystalline and non-crystalline portions and may hinder a growth of the crystallites to larger sizes needed for a reliable molecular structure determination by scattering techniques.

Table 6a. Density of cellulose acetate of various degree of substitution obtained by deacetylation of CTA from different sources using tetrachloride as medium for density investigations [46].

acetyl %	observed density /g cm^{-3}	acetyl %	observed density / g cm^{-3}
44.0	1.288	38.3	1.315
43.4	1.289	33.0	1.346
43.3	1.287	23.7	1.373
40.8	1.304	22.6	1.375
40.5	1.304	17.8	1.426
40.3	1.306	17.3	1.415
39.3	1.311	16.8	1.433
38.4	1.314	16.7	1.417
		14.9	1.445

Table 6b. Density of secondary CA plastics in dependence of plasticizer (ISO R1183) [73].

content of plasticizer / mass %	density / g cm^{-3}
22	1.28
27	1.27
32	1.26

The density of cellulose acetate of various degree of substitution is a remarkable property as it increases linearly with decreasing acetyl content and can be extrapolated to 1.52 g/cm^3 for zero acetyl content (Table 6a). This value agrees with the density of regenerated cellulose II. The observed density for CTA [46] agrees with the one calculated from the unit cell content of CTA II (cf. Table 5) but its increase towards the less crystalline 2.5 and 2.0 CAc is unusual. Since the crystalline part of these specimens exhibit the crystal structure of CTA, the non-crystalline portion possesses a higher density than the crystalline one. Hydrogen bonding between the chains and water uptake seem to be responsible for this unusual non-crystalline, cellulose-like arrangement. Adding plasticizer lowers the density (Table 6b) and creates space for facile motion of the chains i.e. the glass transition deceases as will be discussed in the following section.

It should be pointed out that the model for chain arrangement as depicted in Fig. 15 allows many metastable structures of oriented molecules depending on the rotational position and the relative shift of the chain molecules as well as on the side chain placements. Most of the CAc specimens with low acetyl content will not show crystalline order, which requires three-dimensional periodicity rather than orientation correlation only as experienced in liquid crystals. Such metastable structures have been documented by X-ray patterns by many authors but they are difficult to evaluate, since they do not represent equilibrium states and are dependent on the pretreatment of the samples as well as on the distribution of acetyls groups along the chain, quantities that are often not provided. In addition solvent molecules may be incorporated into the structure. These facts influence the properties of CAc and lead to conflicting experimental results and make a discussion of data provided rather difficult.

4.1.4 Thermal Properties

The melting temperature for crystalline polymers and the glass transition temperature for amorphous and non-crystalline materials are important quantities for processing. On the other side further properties related to temperatures may be needed to describe the handling of materials depending on the brittleness or toughness of the materials. Since melting is a first order equilibrium transition with abrupt enthalpy changes, it can be easily detected by calorimetry as DSC (differential scanning calorimetry) or DTA (differential thermal analysis) or comparable methods. The glass transition is a non-equilibrium transition and depends on the pretreatment of the materials and is related to the onset of segmental chain motion in a polymer but differs from a second order equilibrium transition. The glass transition temperature can be recorded by DSC as a change of specific heat or by DMTA (dynamic mechanical thermal analysis) as a big drop in storage modulus or a peak in the loss modulus. With this technique further motions of the chain molecule (side group, plasticizer etc.) may be detected for an evaluation of the viscoelastic property of polymers.

4.1.4.1 Static Measurements (DSC, etc.)

In general cellulose short side group triesters can be described as polymers with high melting temperatures and low melting entropies, which suggest that in the melt cellulose esters exist as semi-flexible, extended chains supporting the topology proposed in Fig. 15. The thermal data for cellulose triacetate CTA are depicted in Fig. 16 as obtained by TGA (thermal gravimetric analysis, weight loss), DTA and TBA (torsional braid analysis; testing of thin films) [47] that actually represents a dynamic method and added for reasons of comparison. The glass transition temperature from TBA determined to T_g = 172 °C agrees with the one obtained from dilatometry [48]. The melting point is detected at T_m = 307 °C. The DTA curve exhibits a melting temperature T_m = 290 °C and three transition temperatures between 186 and 213 °C, which cannot be explained. Also specific volume measurements of CTA suggest three transitions at 40, 120, 155 °C that do not influence the mechanical properties [49]. The narrow interval between the melting and decomposition temperature (T_d = 356 °C, TGA) as shown in Fig. 16 limits the processing of cellulose triacetate from the melt.

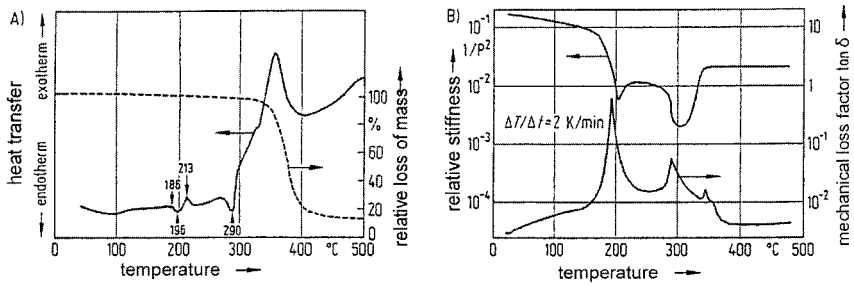

Fig. 16. Thermal investigations of cellulose triacetate in N_2 atmosphere. A: by DTA and TGA; B: by TBA (from [47]).

The thermal data greatly vary for different materials, methods of preparation and analysis. Therefore, an investigation has been undertaken with laboratory prepared cellulose acetates under defined conditions [50]. CTA was produced from purified cotton cellulose by acetylation in an acetic anhydride - acetic acid - sulphuric acid system at 90 °C for an hour, which resulted in a clear and highly viscous reaction mixture. The hydrolysis of CTA to obtain cellulose secondary CA was conducted at an elevated temperature of about 120 °C for about 10-20 min. The DSC thermograms are shown in Fig. 17 with a heating rate of 20 °C /min in a nitrogen atmosphere.

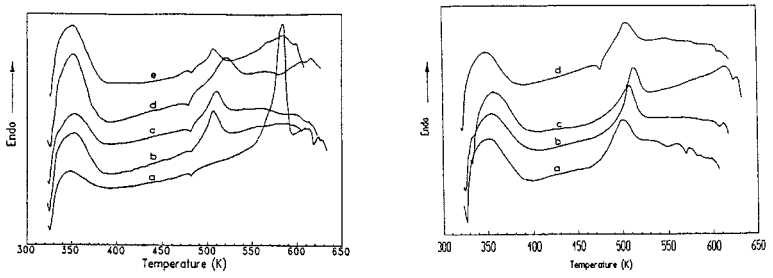

Fig. 17. DSC thermograms of cellulose acetate of various acetic acid content. A: curve a: CTA (61%); b: CA (56.2%); c: CA (54.8%); d: CA (54.5%); e: CA (52.6%);
B: comparison of secondary CA prepared in the laboratory: curve a: 51.6%, d: 54.7% with commercial products by Daicel b: 54.5% and by Celanese c: 54.8% (from [50]).

It is well accepted that crystalline cellulose acetates of various degrees of acetylation show

transitions between 190 and 220 °C (cf. Fig. 16 A), and an endothermic hump is observed between 50 and 80 °C in Fig. 17. This hump lies at the onset of the measurement and is difficult to evaluate. A comparison with DSC data [51] (cf. Fig.21) suggests that evaporation of water may cause this hump. The exothermic peak at 470 to 480 K is assigned to the crystallization temperature T_c of CTA. A pronounced glass transition was not detected in all these samples. The thermograms also provide evidence that the melting temperature and the crystallinity drops considerably for secondary CA due to less perfect and smaller CTA crystallites that are confirmed by X-ray analysis. The T_c peak is not present for commercial samples and the cause is subject to speculations. Differences of the two classes of specimens are manifold from variations in the distribution of trisubstituted anhydroglucopyranose units to remaining residuals from the acetylation and deacetylation process or the hindrance of the crystallization process by fixed molecular sites. X-ray diffraction experiments led to the conclusion that the crystal structure of all the samples belongs to the CTA II type.

An extensive investigation of thermal properties of cellulose acetate with DS of 0.49, 1.75, 2.46 and 2.92 was published by Kamide and Saito [44]. The original specimens and fractionated samples range from $47x10^3$ to $583x10^3$ D in molecular weight for CTA and somewhat smaller for the other CAc with a polydispersity M_w/ M_n of about 1.3 for the fractions. The drop of the baseline just ahead of the crystallization peak was taken as glass transition in DSC experiments (heating rate 10 K/min) of dried samples. A T_g value of 460 K was obtained for the original specimen of CTA. The molecular weight dependence of T_g for the fractions is relatively small with an increase from 460 K for low molecular weight to a constant value of 467 K for M_v (intrinsic viscosity value) > $350x10^3$ D. X-ray investigations on medium molecular weight fractions confirm that the peak directly succeeding the glass transition is caused by crystallization with T_c = 478 K in the DSC thermogram. Crystallinity of the materials disappeared at the DSC peak temperature (melting point) of T_m = 564 K. CTA II modification was established in the crystalline state. The exothermic peak at T_c did not appear again after cooling the samples at 10 K/min to room temperature and also on succeeding heating cycles.

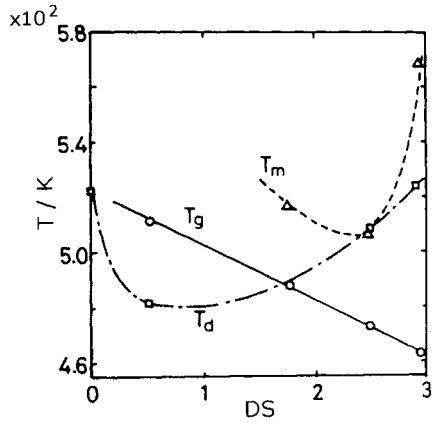

Fig. 18. Dependence of glass transition temperature T_g, melting temperature T_m and decomposition temperature T_d on the average degree of substitution DS (from [44]).

The dependence of T_g, T_m determined by DSC and of the decomposition temperature T_d by TGA on the degree of substitution DS is depicted in Fig. 18. It should be noted that T_g is almost independent on molecular weight and T_d might increase with molecular weight by about 5 %. However, the melting temperature cannot be described in simple terms. Although T_m is almost independent of molecular weight for the original specimens and the fractions, except for DS = 0.49, which does not show any melting, a second endothermic peak appeared for DS 2.46 at 520 K besides a first one at 500 – 510 K. Other researchers have confirmed these findings of two and sometimes even more peaks.

The linear line in Fig.18 for the dependence of the glass transition temperature on the average degree of substitution DS can be described by:

$$T_g(K) = 523 - 20.3\ DS \qquad (2)$$

T_m and T_d show a minimum at DS ~2.5 and ~1, respectively. The DS dependence of the decomposition temperature T_d suggests that the molecular interactions of the chains influence the thermal degradation as well as the conditions and purity of the samples. The starting point of decomposition has been stated as low as 160 °C for secondary CA by some investigations.

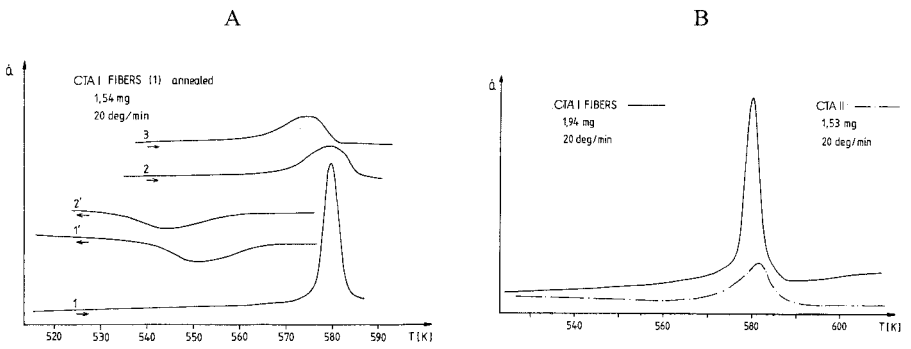

Fig. 19. DSC thermograms of (A) three heating and two cooling cycles (20 K/min) of an original CTA I fiber annealed at 500 K for 30 min and (B) the comparison of heating of a CTA I fiber and CTA II powder.

A distinction between the two crystal structures, CTA I and CTA II, cannot be provided by DSC experiments and have to rely on X-ray diffraction, e.g. the fingerprint method. Excellent DSC-thermograms can be obtained for annealed CTA I fibers with a relatively sharp melting peak at 580 K (Fig. 19) [52]. The second heating cycle exhibits a broad melting peak at about the same temperature. Examination by X-ray diffraction reveals that the sample is transformed to CTA II after cooling down from a few degrees above the melting range. The third heating results in a drop of the melting temperature, which suggests that the crystallization has not been completed, and only small crystallites have been formed. Cyclic cooling leads to a drop of about 30 K and 40 K for the crystallization temperature for the first and second cooling, respectively. Comparison between CTA I and an annealed powder of CTA II shows a small but not significant increase in peak temperature (Fig. 19B).

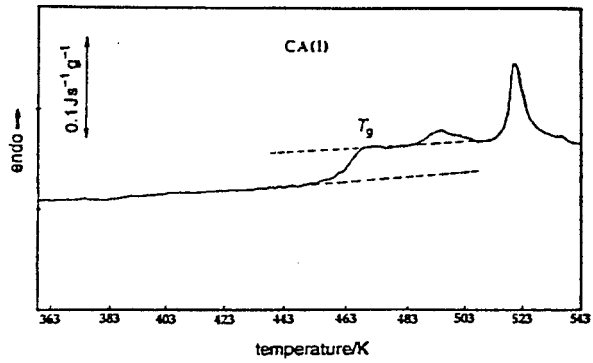

Fig. 20. DSC thermogram for unplasticized, powdered secondary cellulose acetate CA(I). Heating rate 10 K/min (from [51]).

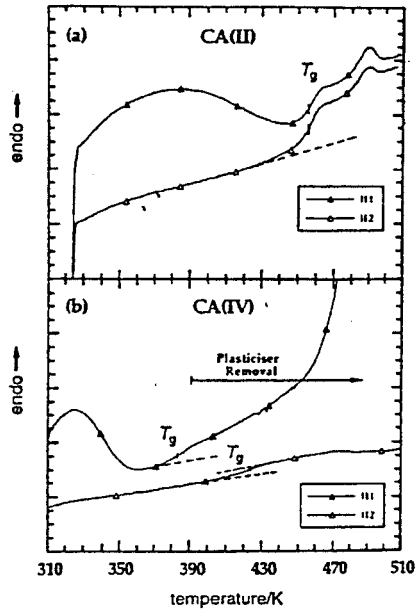

Fig. 21. DSC thermograms showing a) the removal of water and b) the removal of plasticizer with increasing temperature (H1 first heating, H2 second heating). CA(II) pressed secondary CA(I) into sheets at 528 K; secondary CA(IV) with 26 wt% diethylphthalate (DEP) plasticizer; heating rate 10 K/min (from [51]).

In studying the hydration and plasticization effects in secondary cellulose acetates with various methods, including DSC [51], the glass to rubber transition was found at 463 K for secondary CA without plasticizer (cf. Fig. 20), which agrees with the values given above, and DMTA measurements (cf. next section) [53]. At higher temperature melting occurs and ultimately decomposition. Two melting peaks of different size are also shown in Fig. 20 but with a reverse ratio as found in the previously discussed paper [44]. The loss of water in the temperature range of 290-373 K and the loss of plasticizer is depicted in Fig. 21 as the samples are thermally cycled up to 500 K. The thermograms of the second cycle miss the humps, which are caused by water uptake or plasticizer. The plasticizer removal starts at about 390 K.

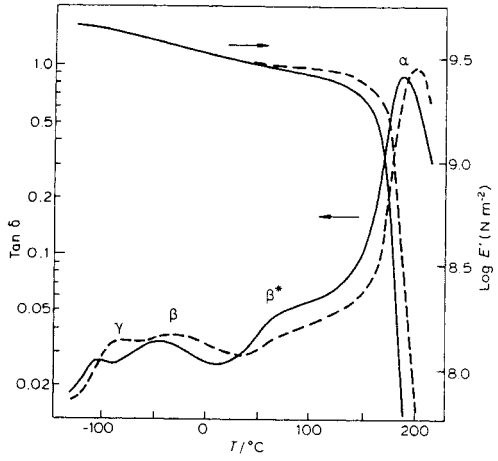

Fig. 22. DMTA spectra of CA (DS = 2.4) at two frequencies: — 0.3 Hz, ---- 30 Hz (from [53]).

4.1.4.2 Dynamic Measurements (DMTA, etc.)

The evaluation of the dynamic modulus by dynamic mechanical thermal analysis DMTA as a function of temperature or frequency leads to a well determined glass transition temperatures, to the stiffness of the materials over a wide temperature range and to ideas about internal motions in materials important for their application, since absorption and dissipation of energy hinders the cracking and breaking of materials.

A DMTA diagram is represented in Fig. 22 for viscoelastic cellulose acetate with a DS of 2.4 at

two frequencies [53]. The storage modulus E' represents the stored elastic energy and the damping factor tan δ = E''/E' shows a more resolved curve of the loss modulus E'', responsible for the dissipation of energy. The decrease of E' mirrors the change in stiffness to lower values with higher temperatures until a steep frequency dependent drop occurs at the glass transition temperature T_g. An extrapolation to zero frequency results in the glass transition temperature as determined by DSC experiments. The changes in storage modulus appear more pronounced as peaks in the loss modulus or in tan δ. The peaks from higher to lower temperature are denoted α, β* (shoulder), β and γ.

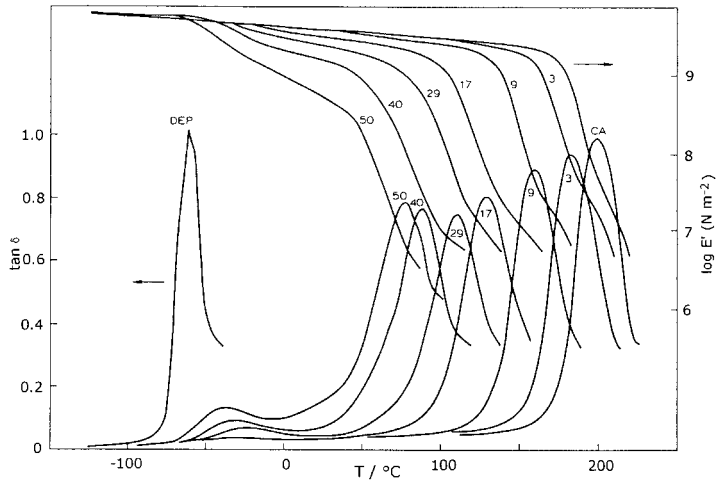

Fig. 23. Storage modulus and damping factor of dynamic mechanical investigations on secondary CA/ diethylphthalate (DEP, plasticizer) of various ratios provided in the figure (from [54]).

The α relaxation or α process corresponds to the glass transition representing the onset of segmental motion and occurs at 197 °C for 3 Hz agreeing well with T_g of ca. 200 °C as calculated by equation (2) as well as the value of 190 °C derived from the trace in Fig. 20. Adding compatible plasticizers suitable for 2.3-2.5 CA, predominantly esters of phthalic acid as diethylphthalate DEP, shift the α relaxation and decrease the stiffness of the materials in the ambient temperature range depending on the amount of plasticizer as shown in Fig. 23 [54]. (A list of commonly used plasticizer can be found in Chapter 5.3, Table 2 of this book.) The glass transition of DEP lies at –63 °C and since only one T_g is present between the ones of secondary

CA and DEP, an intimate interaction can be concluded for this system. Agreement between the DSC (cf. Fig. 21) and DMTA values are evident but it should be noted that the plasticizer evaporates at temperatures slightly above the α relaxation temperature and therefore, a macromolecular plasticizer would be advantageous. An investigation [55] of CAc with DMTA at various DS shows a decrease of T_g with higher DS in agreement with eq. (2). It was also found that higher crystallinity lowers the peak height of the damping factor.

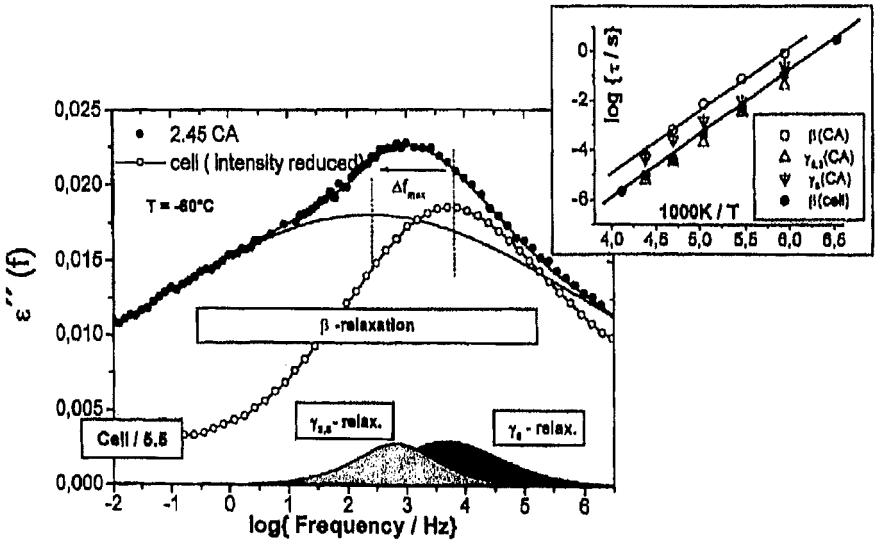

Fig. 24. Dielectric loss spectrum of commercial 2.45 cellulose acetate in comparison with cellulose at –60 °C (from [57]).

The β* shoulder in Fig. 22 is caused by the loss of heterogeneously distributed but bound water and disappears by drying the sample. Irrespective of DS the samples adsorb some humidity when stored at normal room conditions. Different views have been presented for the β and γ relaxation. The β relaxation may be interpreted as a motion of single monomeric units. The peak site does not change with different DS [55, 56] and is also present in dielectric spectra of pure cellulose (cf. Fig. 25). But the β relaxation might well represent a superposition with further contributions as cooperative motions involving side groups and main chain. In DMTA experiments the γ

relaxation vanishes, if completely dried specimens were used and has been related to the onset of motion of loosely bound water.

Dielectric relaxation spectroscopy DRS can also be used to investigate molecular motions in the wide time scale of 0.1 ns -100 s, but only if changes of dipoles in motions occur. In this respect the above discussed β and γ relaxations as well as the effect of water can be detected and additional information gathered with regard to calorimetry (DSC, etc.) and DMTA. The frequencies in DRS spectra can be converted to temperature. Higher frequencies correspond to lower temperatures, the scale being dependent on the interaction energy. The disadvantage of relaxation methods lies in the broad peaks over several decades in frequencies or over a broad range of temperatures. Therefore, it is often difficult to interpret the spectra with regard to specific motions especially of the side groups.

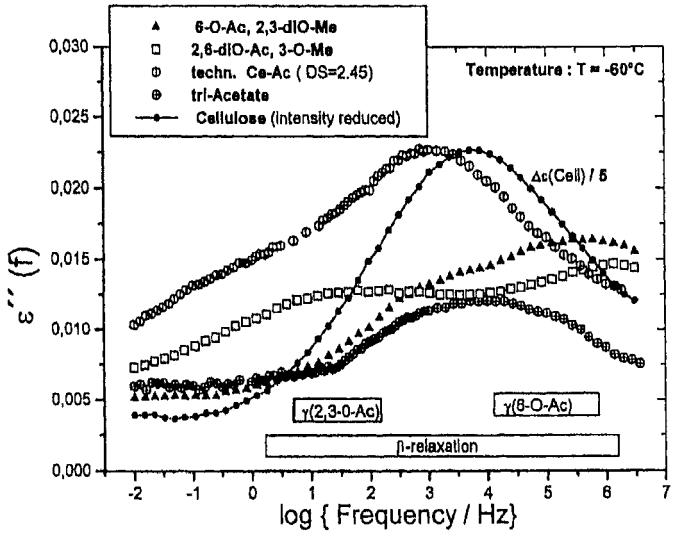

Fig. 25. Dielectric loss spectra of various regioselectively substituted cellulose acetates as indicated in the insert at –60 °C (from [57]).

In an overview of DRS on cellulosics and amylosics, Einfeldt et al. studied secondary CA and compared the spectra with some regioselectively substituted compounds and came to new insights [57]. Fig. 24 addresses a frequency range with superimposed relaxations: the β relaxation (motion

of a monomeric unit), the γ_s relaxation of the O6 side group (side group rotation) and the overlapping γ_s relaxations of the O2, O3 side groups. The term γ_s is used, since this relaxation does not correspond to the γ relaxation of DMTA investigations rather relates to the proposed side group motion underlying the β peak. This assignment is confirmed by the dielectric loss spectra in Fig. 25 of regioselectively substituted compounds for which the γ_s relaxations are missing when the corresponding acetyl side group is absent. The inserted diagram in Fig. 24 suggests an Arrhenius type of process, since the log τ (T) plotted over 1/T results in a straight line. The activation energy can be determined from the slope. The relaxation time τ was taken as the inverse of $2\pi\nu$, the frequency of the peak maximum. All the processes considered in the insert lead to almost the same activation energy.

4.1.5 Mechanical Properties

The basis of the mechanical characterization and properties for CAc will be addressed for fibers, films and plastics, leaving these and further features for membranes, composites, coatings etc. to further chapters in this book or the general literature.

The stress–strain relationship for larger elongations as well as the stress–temperature (or modulus-frequency) relationship at small elongations, including the above discussed DMTA investigations, provide insight into the materials properties. Various representations of stress-strain curves are found [58], and therefore, a short introduction of terms and conversions of quantities will be provided and some visualized in Fig. 26. The conversions to SI units are summarized in Appendix A2.

Tex is a useful and appropriate quantity in fiber science and describes the mass in g of a fiber of 1 km in length (1 tex = 1 g/km = 9 den; denier (den) another measure often applied, older papers also use grex as mass in g of a fiber of 10 km in length). The cross section, rather difficult to obtain for long and thin fibers, is not required in the tex representation.

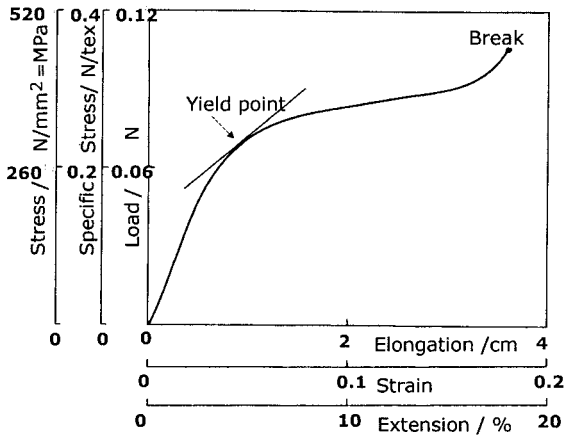

Fig. 26. Stress–strain curve in various representations as found in literature. The following properties were chosen for the specimen: a fiber of length 20 cm, 0.3 tex and density 1.3 g/cm^3 (density value observed for commercial CAc) [58].

The stress f is defined:

stress = load / area of cross section,

load as force in Newton N or as mass in kg. The mass in kg leads to the force in N in the gravitational field of the earth by multiplication with the factor of 9.80665, sometimes this load is expressed by the dimension kgf, signifying a force. The stress is usually expressed in N/mm^2 = MPa. The specific stress σ is often preferred, since no cross section of the fiber is required:

specific stress = load / mass per unit length.

Dimension in the SI system is N m/ kg or usual N/ tex. The following relationship with the density ρ in g/ cm^3 holds:

$$\sigma = f / \rho \qquad (3)$$

The distinction between the two quantities, stress f and specific stress σ is only significant when two materials with different densities are compared.

The strain, often termed tensile strain or percentage of extension, is given by:

strain = elongation / initial length.

The strength of a material is a measure of the steady force necessary to rapture (break) the

material and is defined as the breaking load (maximum load in an experiment; cf. Fig. 26 break point). The value of the specific stress at break is a good quantity for comparing different fibers and is called tenacity or specific strength. Further useful quantities are the elongation at break and the work of rapture, which represents the area below the curve of Fig. 26 from zero elongation to elongation at break with the load given in Newton N. The initial modulus can be derived as the initial slope of the specific stress–strain curve. The yield point is given by the turning of the steep slope of the curve into a shallow one and may exactly be defined by various methods.

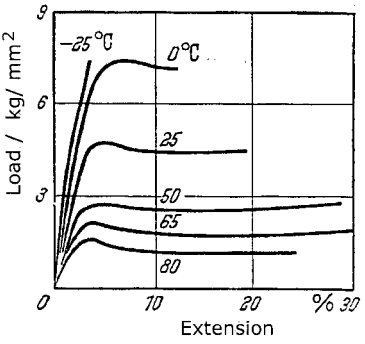

Fig. 27. Influence of temperature on load–extension curves of secondary CA fibers (from [59]).

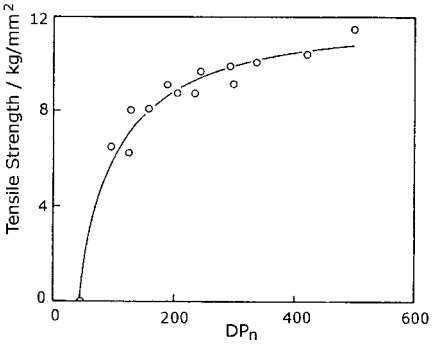

Fig. 28. Influence of DP on tensile strength of secondary CA (from [61]).

The appearance of the stress–strain curves of a certain material will be influenced by the internal mobility of the material that may be triggered and increased by swelling as well as by higher temperatures and lowered by orientation and crystallization. The yield point may be interpreted as the lower limit or starting point of a quasi-permanent deformation, and the slopes of the two branches of the curves represent the modulus of elasticity of the materials at low or high strain. The actual amount of bending of the stress-strain curve at the yield point mirrors an important property for application, since it marks the yield under high loads and influences the handling of fabrics.

Alfrey [60] introduced a classification for various types of materials depending on the shape of the stress–strain curves (Table 7). The stress-strain curve for low temperatures (-25 °C) for secondary CA fibers in Fig. 27 belongs to the type "hard brittle" and for higher temperatures to "soft tough". Besides the temperature, moisture and other swelling agents increase the plastic flow and

influence the shape of the stress-strain curves or the tensile strength besides the degree of polymerization DP (Fig. 28). Another factor to be concerned is the rate of strain or extension applied to the materials tested. At low rates plastic flow may occur and results in a wide yield region and an appreciable extension of break. The same sample may show a steep stress-strain curve, fail to produce any yield region and break at higher strength. Therefore, the pretreatment of the materials, the relative humidity but also the rate of strain and other significant factors should be taken into consideration in testing.

Table 7. Types of materials [60].

Type	elasticity modulus	yield point	extension of flat curve	break point
soft weak	low	low	low	low
soft tough	low	low	high	high
hard brittle	high	not defined	low	medium
hard strong	high	high	medium	high
hard tough	high	high	high	high

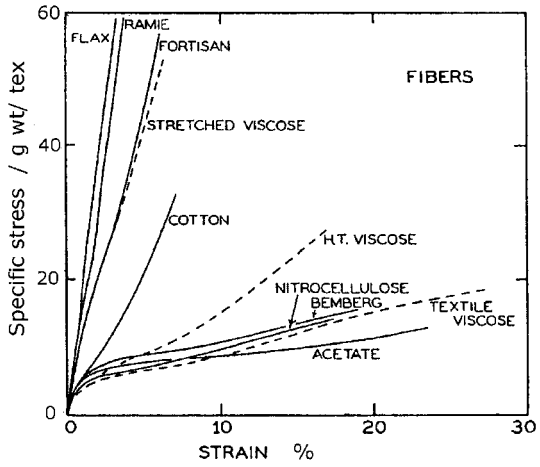

Fig. 29. Stress-strain curves for filaments of typical cellulosic materials (from [62]) at 65% rh, 20 °C; 1 cm filament length, rate of elongation. 90 (gf/ tex)/ min. Fortisan: stretched and saponified acetate filament, HT: high tenacity viscose, Bemberg: continuous filament of cuproammonium rayon.

The inherent mechanical properties of a fiber are described by the stress-strain curve and the recovery behavior under conditions of torsional bending, tensile and shear loading. Stress-strain curves of cellulosic fibers are shown in Fig. 29. It should be emphasized that these curves apply only to particular types of materials and to particular conditions of test.

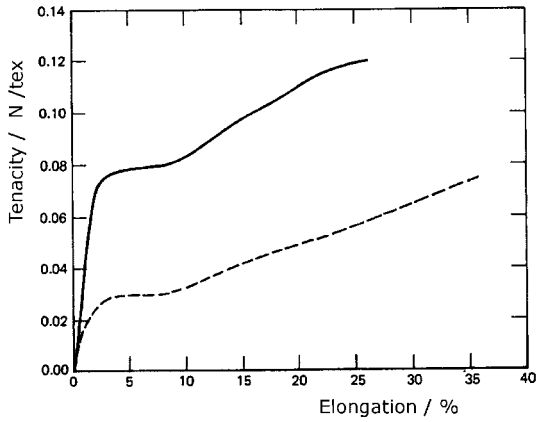

Fig. 30. Typical stress-strain curves for bright cellulose triacetate yarn under standard (upper curve, 65% rh, 21 °C) and wet (lower curve, 21 °C) conditions. Rate of extension 60%/min, 3.9 cm gauge length (from [63]).

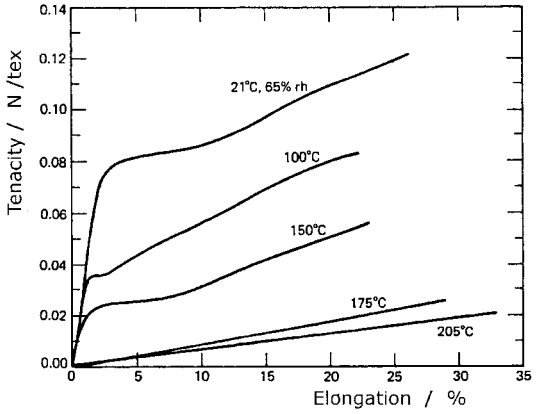

Fig. 31. The effect of temperature on the stress–strain properties of CTA yarn. 60%/min rate of extension, 3.9 cm gauge length (from [63]).

The stress-strain curves of acetate fibers show an initial rapid rise with a marked yield point followed by a nearly flat portion and a further rise as the break point approaches as demonstrated for secondary CA in Fig. 29 and for CTA in Figs. 30 and 31. Temperature and moisture content of the fiber affect the viscoelastic behavior. The effect of moisture on the stress-strain curve of CTA is depicted in Fig. 30 and that of temperature in Fig. 31. Therefore, comparable measurements have to be carried out at standard conditions, which have been chosen as 21 °C and 65% rh. Elongation at break for secondary CA and CTA varies under these conditions (65% rh, 21 °C) from 25-45%, under wet conditions from 35-50% for various specimens.

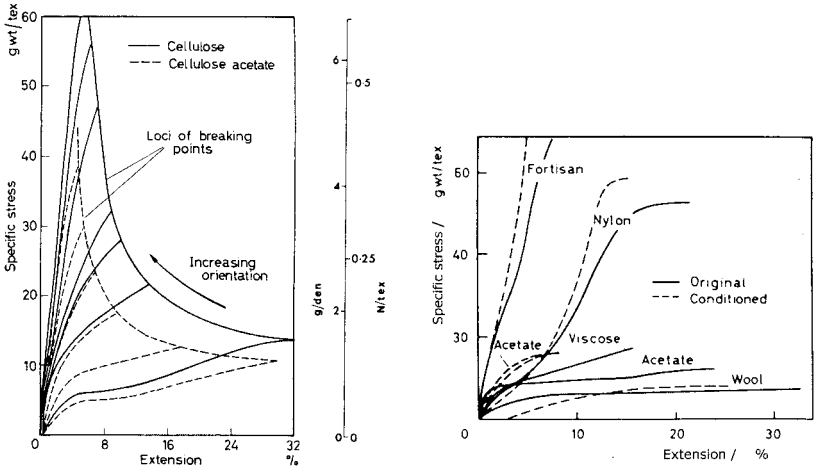

Fig. 32. Stress-strain curves of filaments. Left: Various degrees of orientation (cellulose = regenerated from acetate). The lowest curve in each set is for unoriented materials (from [64]. Right: Before and after repeated (50 cycles) elongation to 80 % of breaking extension (from [65]).

From Fig. 29 it is evident that stretching of fibers causes big differences in the stress strain-curves. Stretched fibers with good molecular orientation exhibit high strength and little extensibility whereas the unstretched fibers are weaker but more extensible as shown in Fig. 32 with practical implications. The properties of fibers may be changed by high force fields during processing or by high strain in use.

The apparent modulus of a viscoelastic fiber or textiles is defined as the ratio of stress to strain in the initial, linear portion of the stress-strain curve and represents the ability of a material to resist

deformation. This modulus of elasticity is related to many of the mechanical performance characteristics of materials. The modulus of elasticity can be affected by drawing the fiber i.e. elongation as well as the internal structure of the fiber including morphology. Commercial secondary CA and CTA can be characterized by 2.2-4.0 N/tex (25-45 g/den). The change of the modulus of dry and wet fibers with temperature is shown in Fig. 33. The ability of a fiber to absorb energy during straining is measured by the area under the stress-strain curve and is known as toughness or work of rapture, which lies for all secondary CA at ca 0.022 N/tex. The ratio of work recovered of the total work absorbed is termed resilience.

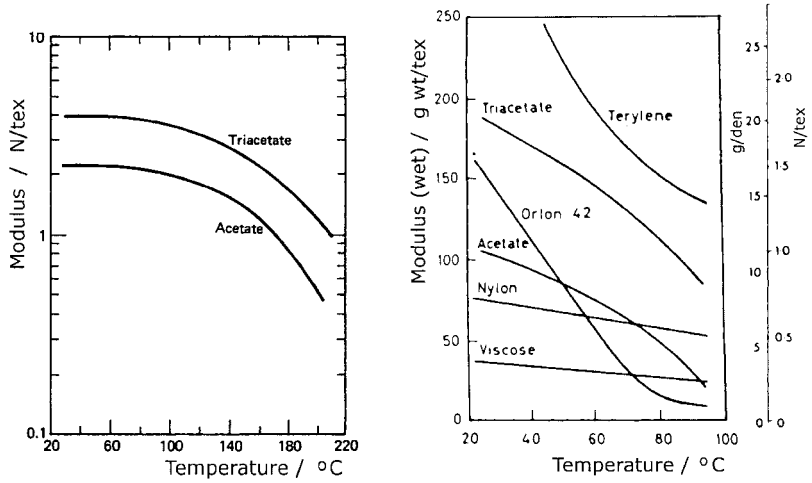

Fig. 33. Tensile modulus as a function of temperature for dry fibers (left picture; from [63]) and wet fibers placed in water (right picture; from [66]).

The dimensional change with time of a material under physical load is called creep (Fig. 34). At room temperature, it is also known as cold flow. Most biologically derived materials are cross-linked and therefore are relatively resistant to creep. Polymers are characterized by a creep-modulus, which is calculated as the secant modulus of creep stress/ creep strain at fixed stress and time. Creep of acetate fibers increase with temperature [67], but also with humidity [68] as depicted in Fig. 35.

Elasticity has been defined by the American Society for Testing and Materials (ASTM) as the "property of a body by virtue of which it tends to recover its original size and shape after

deformation" [58]. Plasticity is its opposite. A deformation may be divided up into an elastic part, which is recovered by removing the stress and a plastic or permanent part as shown schematically in Fig. 36. Elastic recovery may be defined [58]:

elastic recovery = elastic extension/ total extension

or work recovery:

work recovery = work returned during recovery / total work done in extension.

The portion of the total work that is dissipated into heat is given by (1- work recovery).

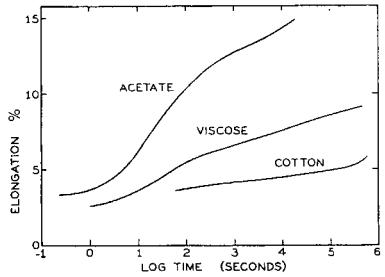

Fig. 34. Creep curves for cellulosic fibers at 65 % rh, 21 °C under stress of $9x10^3$ N/cm^2 (from [61]).

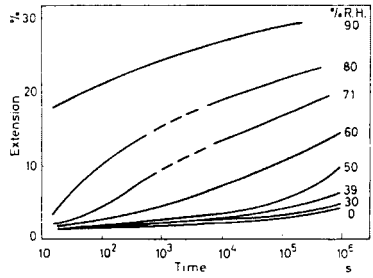

Fig. 35. Effect of humidity on creep of secondary CA (from [68]).

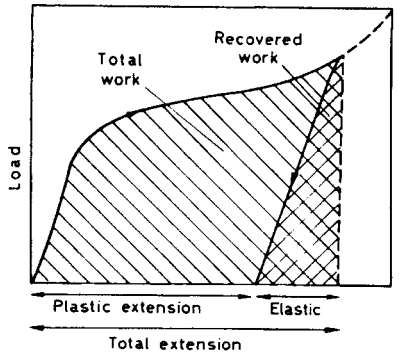

Fig. 36. Typical stress-strain curve to identify elastic and plastic extension (from [58]).

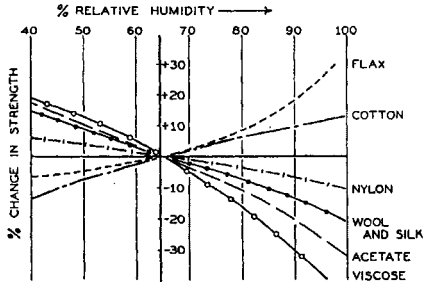

Fig. 37. Relative change in strength with humidity for various fibers (from [69]).

4.1.6 Sorption

The absorption of moisture by the fibers depends on the relative humidity to which the fibers are exposed and it changes the strength of the fibers (cf. Fig. 37). The moisture content varies depending if the equilibrium is approached from the dry or wet side as shown in Fig. 38. Heat treatment of the fibers before the exposure limits the values to 2.5-3.2 % for CTA.

The moisture regain of cellulose triesters decreases with increasing size of the substituent and reaches a minimum with triheptanoate after which a slight increase occurs [70]. A remarkable relation exists between the DS and moisture regain of cellulose acetate depending on the method of preparation. A linear decrease with increasing DS was reported for heterogeneously prepared acetates but homogeneous acetylation yields acetates of higher moisture regain and first an increase and than a decrease with DS as depicted in Fig. 39. For higher DS these curves meet the ones for heterogeneously derived acetate.

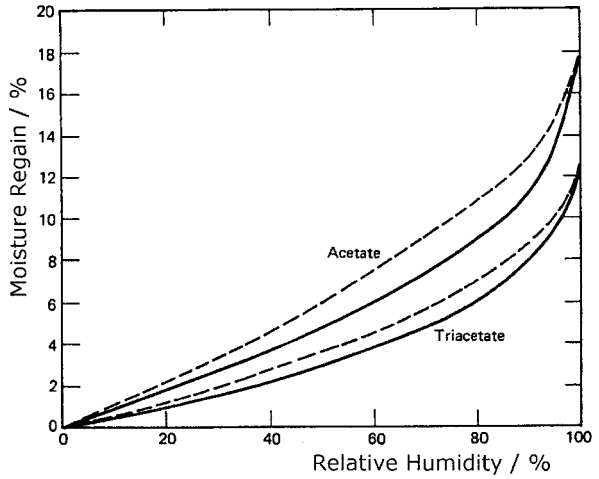

Fig. 38. Moisture regain (moisture content on a bone-dry basis) of secondary CA and CTA fibers on absorption (lower curves) and desorption (upper curves) at 22 °C (from [63]).

The moisture regain of cellulose derivatives is dependent on the nature of substituents, the degree of substitution and their distribution along the chain as well as the extent of crystallization but independent on the molecular weight. The moisture regain increases with decreasing crystallinity. The introduction of statistically distributed side groups in a homogeneous reaction will block the

access of adjacent hydroxyl groups to form hydrogen bonds and prevents crystallization. The increase of moisture sorption (cf. Fig. 39) at low DS is proportional to the availability of hydroxyls for water sorption but at higher DS there are less hydroxyls available causing a decrease of sorption. At high DS some deviation also occurs from linearity. In heterogeneous reactions different effects govern the acetylation process. At the beginning of the reaction the inaccessible crystalline regions are only slightly affected. The substitution starts immediately in accessible regions with almost simultaneous reaction of the freed hydroxyl groups. The decrease of moisture sorption arises from the decrease of the number of hydroxyl groups which are not available to water molecules.

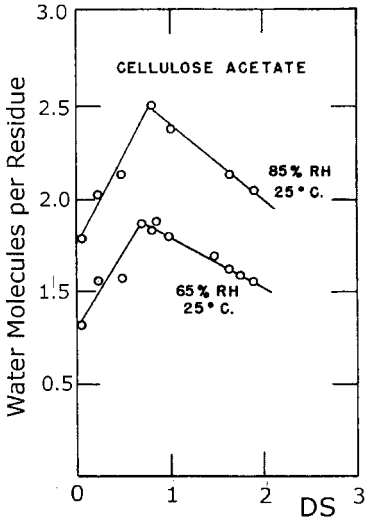

Fig. 39. Variation of moisture regain of homogeneous CAc with DS (from [71]).

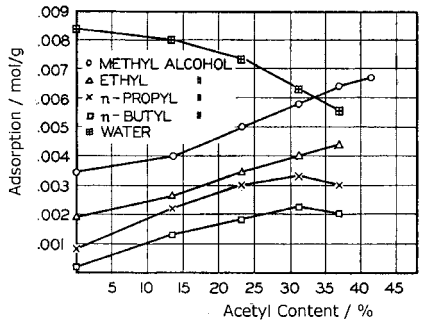

Fig. 40. Adsorption of alcohols by CAc as a function of acetyl content (from [72]).

In Fig. 40 the results of adsorption on CAc with increasing DS are presented for alcohols with various chain lengths. It can be concluded that at low DS the interaction of adsorbed molecules with the hydroxyl groups of cellulose contribute most to sorption but with increasing DS the alkyl groups yield an increasing contribution to the sorption.

Water uptake causes swelling of fibers, roughly proportional to the moisture content, for secondary CA ca. 1% in length and 10% in cross section, for CTA 4% in cross section and 1.5%

for heat-treated samples. At the initial stage of adsorption, the total volume of the system is less than the volume of the dry fiber and the adsorbed water, resulting in an increase of density. Therefore, care has to be taken if densities are measured with water present in immersion liquids. Swelling of filaments at high humidity or in water cannot directly be related to the non-crystalline state of materials present. Qualitatively, the observed swelling can be explained on the basis of variation in lateral order distribution. Morphologies comprised of small ordered regions and small disordered regions would be expected to swell less in water than ones comprised of large ordered regions separated by large disordered regions. These small regions may contribute little to crystallinity but will affect swelling in much the same manner as a chemical cross-linking.

4.1.7 Quality Control and Testing

In the following section properties will be introduced for quality control and testing as well as for evaluating cellulose acetate for specific commercial application. Such properties are generally collected in data sheets published by the suppliers.

Most of the commercially produced cellulose acetate (reference years 1982 - 1985) is consumed as triacetate CTA in textile fibers (280 10^3 t/a), films for photography (60 10^3 t/a) and secondary acetate as filter tow for cigarettes (370 10^3 t/a), thermoplastic products and foils (50 10^3 t/a) [73].

The chirality of the cellulose molecules, an extraordinary feature, has been utilized when enantiomeric separation of chiral compounds are conducted in liquid chromatography columns using as stationary phase either coated silica beats or heterogeneously derivatized microcrystalline materials (cf. Chapter 5.6). Additional application for cellulose acetate as membrane material, hollow fibers or as electrically insulating foils as well as modern coatings, controlled release of activates should be mentioned.

Secondary cellulose acetate CA fibers have a low degree of crystallinity and orientation even after heat treatment whereas CTA exhibits many improved features from a considerable increase of crystallinity after heat treatment. Both cellulose acetates have a bright, lustrous appearance, which can be improved in a duller, whiter yarn by the addition of 1-2% of titanium dioxide or other pigments.

The density of fibers is difficult to measure due to an irregular fiber cross section. The following values are commonly accepted: 1.33 g cm^{-3} (older literature value 1.294) for molding plastics and

fibers of secondary CA and 1.30 g cm^{-3} for CTA with 55 and 61.5% acetic acid content (cf. also Table 6).

Colored secondary CA and CTA yarns are produced by incorporating colored pigments, soluble dyes or carbon in the polymer solution before extrusion. These yarns are extremely colorfast to all kind of treatment as washing etc.

Optical Properties

Secondary CA and CTA show very small light scattering (< 0.5 cd/ mm^2 lx at 2mm thickness) determined for molding plastics, which compare with window glass in the visible light range (Fig. 41). Mixing in UV absorber may reduce the high transmission for UV light. The refractive index reaches about 1.48 depending on plasticizer, and fibers show a slight birefringence that is almost undetectable in CTA [73].

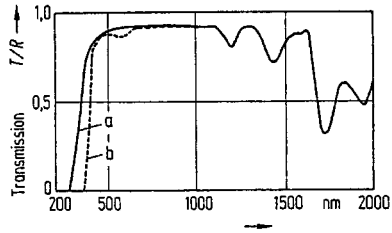

Fig. 41. Transmission of light by clear cellulose acetate propionate plastics (CAP) of 2 mm thickness without (a) and with (b) UV absorber added. Valid also for all CAc and CAB (cellulose acetate butyrate; from [73]).

Thermal properties

Properties to describe the thermal behavior are the sticking, softening and melting. The sticking and softening temperature for fibers rely besides the melting behavior on yarn diameter, fabric construction and general geometry and are found for secondary CA in the 190-205 °C range, fusion at ca. 260 °C. The apparent shining temperature is usually less than the sticking temperature, which leads to the recommendation that the sole temperature of an iron should not exceed 170-180 °C but for heat treated CTA this temperature might be considerably higher, of which the melting point is found to be about 300 °C.

The Vicat-temperature describes the softening of plastic by a standard test: The sample is heated up in an oil bath with a constant heating rate while a point load is applied. The temperature is

recorded, at which the needle with a point of 1 mm^2 penetrates the material 1 mm (ISO 306; DIN 53460 and ASTM D1525 are comparable). Vicat-A: load 9.81 N, Vicat-B: 49.05 N.
The heat deflection temperature (HDT) describes the temperature at which a specific bending of materials occurs by heating with a constant rate under a constant load (ISO 75; DIN 53461 and ASTM D648 comparable). HDT-A: load 1.80 N/mm^2, HDT-B: load 0.45 N/mm^2.

Melt Flow Index (MFI) - Melt Flow Rate (MFR) (ISO 1133; ASTM D1238, DIN 53735)
The melt flow rate measures the rate of extrusion of thermoplastics through a heated orifice and a load placed upon specified for the material. The molten material is forced through the die. A timed extrudate is collected and weighed. Melt flow rate values are calculated in g/10 min. This test provides a means of measuring flow of a melted material, which can be used to differentiate grades of polymers or determine the extent of degradation of the plastic as a result of molding. Degraded materials will generally flow more easily as a result of reduced molecular weight and may exhibit reduced physical properties. The melt flow rate or index is primarily determined by the average molecular weight and is used as tool for quality control. ASTM and ISO vary somewhat in test procedure, but provide similar results.

Flammability UL 94
The most widely accepted flammability performance standards for plastic materials are UL 94 ratings. These are intended to provide an indication of the ability of a material to extinguish a flame, once ignited. Several ratings can be applied based on the rate of burning, time to extinguish, ability to resist dripping, and whether or not drips are burning. Each material tested may receive several ratings based on color and/or thickness. When specifying a material for an application, the UL rating should be applicable for the thickness used in the wall section in the plastic part. The UL rating should always be reported with the thickness; just reporting the UL rating without mentioning thickness is insufficient.

Limited Oxygen Index (ASTM D2863, ISO 4589)
The purpose of the oxygen index test is to measure the relative flammability of materials by burning them in a controlled environment. The oxygen index represents the minimum level of oxygen in the atmosphere, which can sustain flame on a thermoplastic material. The test

atmosphere is an externally controlled mixture of nitrogen and oxygen. A supported specimen is ignited with a pilot flame, which is then removed. In successive test runs, the oxygen concentration is reduced to a point where the sample can no longer support combustion. Limited Oxygen Index or LOI is defined as the minimum oxygen concentration, in which the material will burn for three minutes or can keep the sample burning over a distance of 50 mm. The higher the LOI value, the less is the likelihood of combustion.

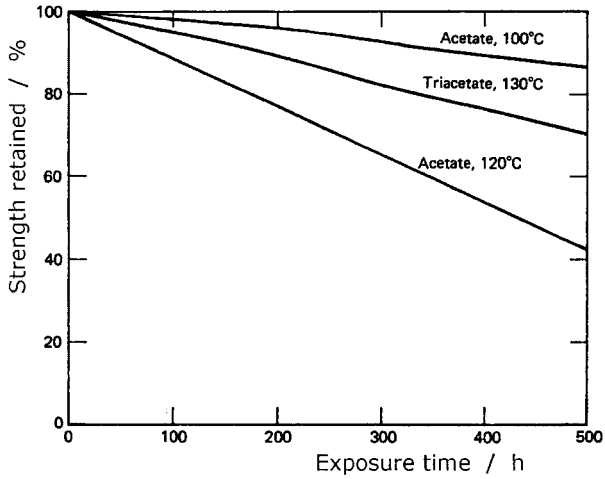

Fig. 42. Effect of dry heat exposure on secondary CA and CTA yarn lubricant free (60% rh, 21 °C) (from [63]).

Mechanical Properties

Moderate changes occur in mechanical properties, e.g. the tensile modulus decreases with temperature as shown in Fig. 33 and the secondary CA and CTA fibers extend more rapidly under stress and are weekend by longer exposure at elevated temperatures in air (Fig. 42).

Hardness Properties

Standard test for hardness imply two different methods. The Rockwell hardness test determines the hardness of plastics after allowing for elastic recovery of the test specimen. This is different from both Ball and Shore hardness: in these tests, hardness is derived from the depth of penetration under load, thus excluding any elastic recovery of the material. Therefore, Rockwell

values cannot be directly related to Ball or Shore values.

Ranges for Shore A and D values can be compared to ranges for Ball indentation hardness values. A linear correlation, however, does not exist.

Ball Hardness

A polished hardened steel ball with a diameter of 5 mm is pressed into the surface of a test specimen (at least 4 mm thick) with a force of 358 Newton (ISO 2039-1). After 30 seconds of load application, the depth of the impression is measured, from which the surface area of the impression is calculated. Ball hardness H358/30 is calculated as applied load divided by surface area of impression. Results are reported in N/mm^2.

Rockwell Hardness (ISO 2939; ASTM D785)

The Rockwell hardness test method consists of indenting the test material with a diamond cone or hardened steel ball indenter. The indenter is forced into the test material under a preliminary minor load usually 10 kgf. When equilibrium has been reached, an indicating device, which follows the movements of the indenter and so responds to changes in depth of penetration of the indenter, is set to a datum position. While the preliminary minor load is still applied, an additional major load is applied with resulting increase in penetration. When equilibrium has again been reached, the additional major load is removed but the preliminary minor load is still maintained. Removal of the additional major load allows a partial recovery and reduces the depth of penetration. The permanent increase in depth of penetration, resulting from the application and removal of the additional major load is used to calculate the Rockwell hardness number HR.

Impact Properties

In standard testing, such as tensile and flexural testing, the material absorbs energy slowly. In real life, materials often absorb applied forces very quickly: falling objects, blows, collisions, drops, etc. The purpose of impact testing is to simulate these conditions. Izod and Charpy methods are used to investigate the behavior of specified specimens under specified impact stresses, and to estimate the brittleness or toughness of specimens. They should not be used as a source of data for design calculations on components. Information on the typical behavior of a material can be obtained by using different types of test specimens prepared under different conditions, varying

notch radius and test temperatures.

Both tests are performed on a pendulum impact machine. The specimen is clamped in a vice; the pendulum hammer - with a hardened steel striking edge with specified radius - is released from a predefined height, causing the specimen to shear from the sudden load. The residual energy in the pendulum hammer carries it upwards: the difference in the drop height and return height represents the energy to break the test bar. The test can be carried out at room temperature, or at lower temperatures to test cold-temperature embrittlement. Test bars can vary in type and in dimensions of the notches.

Izod Impact Strength (ASTM D256 ; ISO180)

The notched Izod impact test has become the standard for comparing the impact resistance of plastic materials. However, this test has little relevance to the response of a molded part to an actual environmental impact. Because of the varying notch sensitivity of materials, this test will penalize some materials more than others. Although they have often been questioned as a meaningful measure of impact resistance - the test tends to measure notch sensitivity rather than the ability of plastic to withstand impact - the values are widely accepted as a guide for comparison of toughness between materials. The notched Izod test is best applied in determining the impact resistance for parts with many sharp corners, such as ribs, intersecting walls and other stress risers. The unnotched Izod test uses the same loading geometry with the exception that there is no notch cut into the specimen (or the specimen is clamped in a reversed way). This type of testing always provides superior values over notched Izod because of the lack of a stress concentrator.

The ISO designation reflects type of specimen and type of notch: ISO 180/1A means specimen type 1 and notch type A. The dimensions of specimen type 1 are 80 mm long, 10 mm high and 4 mm thick. ISO 180/1U (indicating unnotched) means the same type 1 specimen, but clamped in a reversed way. The specimens as used in the ASTM method have similar dimensions, same notch radius and same height, but differ in length: 63.5 mm, and, more importantly, in thickness: 3.2 mm.

The ISO results are defined as the impact energy in joules used to break the test specimen, divided by the specimen area at the notch. Results are reported in kJ/m^2. The ASTM results are defined as the impact energy in joules, divided by the length of the notch (or thickness of the

specimen). They are reported in J/m. The difference in specimen thickness may result in different interpretations of impact strength.

Flexural Strength and Modulus (ASTM D790; equivalent ISO 178 and DIN 53452)

Flexural strength is the measure of how well a material resists bending, or what is the stiffness of the material. In flexural testing all force is applied in one direction. A simple, freely supported beam is loaded at mid-span thereby producing three-point loading. On a standard testing machine, the loading nose is pushed onto the specimen at a constant rate of 2 mm/min. To calculate the flexural modulus, a load deflection curve is plotted using the recorded data. The flexural modulus is determined from the initial linear portion of the curve by using at least five values of load and deflection.

The flexural modulus (ratio of stress to strain) is most often quoted when citing flexural properties. Flexural modulus is equivalent to the slope of the line tangential to the stress-strain curve for the portion of the curve where the plastic has not yet deformed. Values for flexural stress and flexural modulus are reported in MPa (PSI).

Electric properties

CAc as non-metallic organic materials represents good non-conducting properties. Details may be available from manufacturers' information and special publications. Some basic properties are given by a so-called relief diagram that allows the rapid visual assessment of a material (Fig. 43)[74]. The block lengths demonstrate the variation of a certain property.

CTI represents the comparative tracking index that is a suitable property for describing electrical insulation. The numerical value is defined by the voltage that will cause failure by tracking during a standard test after 50 drops of 0.1% ammonium chloride solution have fallen on a material of nominal 3 mm thickness. The results are considered representative of the materials performance at any thickness.

Tracking is the process that produces partially conduction path of localized deterioration of the surface of an insulating material. This is a result of the action of electrical discharges in or close to an insulation surface. Secondary CA is rated by the second highest tracking index, the highest index belongs to the CTI range >600 V.

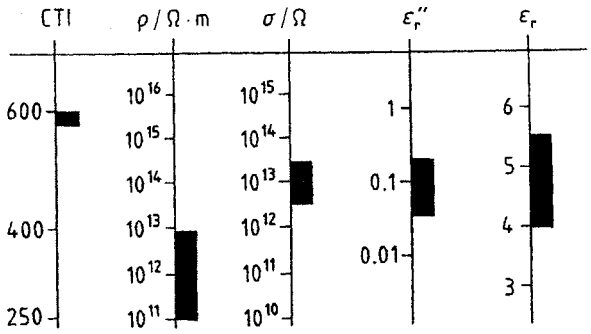

Fig. 43. Relief diagram of electrical properties of cellulose acetate (from [74]).

The volume resistivity ρ, surface resistivity σ (both IEC 93) as well as the relative permittivity ε_r and loss index ε'' (IEC 250 at 1 kHz) are all determined at 23 °C , 50% rh. The surface resistivity represents the ability to resist current flow along the surface of a material, the volume resistivity through the volume. ASTM D257 describes the surface resistivity of surface mounted electrodes of unit width and unit spacing in Ω and the volume resistivity of a unit cube in Ω cm. A material is considered an insulator with a volume resistivity of > 1088 Ω cm.

Secondary CA exhibits antistatic properties despite high electrical resistance, is crystal clear, tough, hard, scratch-resistant, insensitive to stress cracking, readily dye-able with brilliant colors but not permanently weather-resistant and less suitable for precision components. It is used for tool handles, electric insulation films, lights and casings.

Dielectric strength (ASTM D149) reflects the electric strength of insulating materials at power frequencies (48 Hz to 62 Hz) or the measure of dielectric breakdown resistance of a material under an applied voltage. The applied voltage just before breakdown is divided by the specimen thickness to give the value in kV/mm. The surrounding medium can be air or oil. The thickness dependence can be significant. All values are reported at specimen thickness.

Data sheets of various kinds of CAc fibers, films and plastics for application are published by the suppliers for their specific products (cf. example Appendix A3). Some properties for CTA and secondary CA are listed in Table A1 of Appendix A4. Figures and tables for CAc representing standard quality tests as well as dependencies on plasticizer and other variables can be found e.g.

in encyclopedias [75] and handbooks [73]. Data for plasticized films are also presented in Chapter 5.3.

4.1.8 Structures of Cellulosics in Solution

Studies on solution properties of cellulose derivatives reveal two extreme forms of structures in dilute solution. On the one side, molecularly dispersed solutions are present, in which the macromolecules are separated from each other and surrounded by solvent molecules. Such a solution may be obtained when the cellulose molecules are fully substituted and strong polar interactions are excluded between macromolecule and solvent. This type of solution may also be present, if the strong polar bonds are shielded or not effective, e.g. 2.5 substituted derivatives in a homogenous manner with no possibility of strong hydrogen bonding interactions. On the other side, if strong hydrogen bond interactions or incompatible interactions in solution are possible, irreversible aggregation may occur and the molecules cannot not be separated. But we can also expect that the interactions are not strong enough and reversible associations or clusters may be formed. Tools by which these structural models can be investigated rely on molecular mass and geometric shape determination available by static and dynamic light scattering.

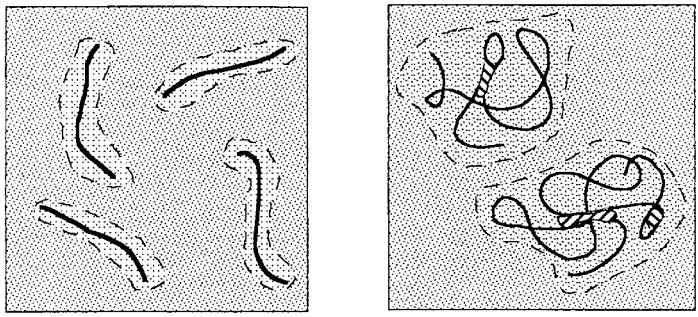

Fig. 44. Schematic representation of single semi-flexible macromolecules in molecularly dispersed dilute solutions. Low molecular mass (left), high molecular mass (right). A solvent shell is indicated by the dashed line (from [76]).

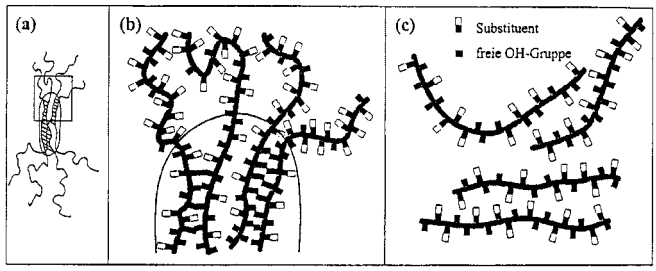

Fig. 45. Schematic representation of aggregation (micelles) in dilute solutions (a); enlarged section of (a) showing blocky distribution of OH and substituents (b); and homogeneous distribution of both groups leading to molecularly dispersed structures (c) (from [77]).

Semi-flexible macromolecules are characterized by a long persistence length as detected for cellulose derivatives. As result the chains resemble rod-like molecules, if only a few persistence lengths long, but exhibit a gaussian coil shape at high molecular mass represented in Fig. 44. Some deviations from the projected shapes may occur, if stronger interactions between segments are possible. A blocky substituent distribution, e.g. in commercial secondary 2.5 acetate, may lead to an irreversible micellar structure with tightly connected segments in dilute solution as schematically represented in Fig. 45 a, b and may contrast a molecularly dispersed solution of a uniform substituent distribution along the chains in Fig. 45 c.

A more detailed discussion has to include the persistence or Kuhn segment length and the interaction with solvent. The models derived from such a study carried out on cellulose -phenylcarbamate, -benzoate, -phenylcarbamate-acetate and -benzoate-acetate are presented for various chain lengths in Fig. 46. These compounds have been synthesized in DMAc/LiCl (N,N-dimethylacetamide/ lithium chloride) considered to produce uniform substituent distribution and dissolved in DMF (N,N-dimetylformamide) or EMMAc (2-methoxyethyleneacetate). The partially substituted cellulose phenylcarbamate and benzoate form molecularly dispersed solution in DMF as well as the fully substituted and the non-fully substituted ones after peracetylation. In EMMAc a longer Kuhn segment length was detected, and in addition the apparent molecular mass was increased to 1.5 times the original one as determined in DMF. Some molecules may form duplex structures in EMMAc as shown in Fig. 46a with a doubling of the molecular mass but an average molar mass of 1.5 of the original one will be obtained when all molecules are

considered. Here, the beginning of aggregation or association can be established.

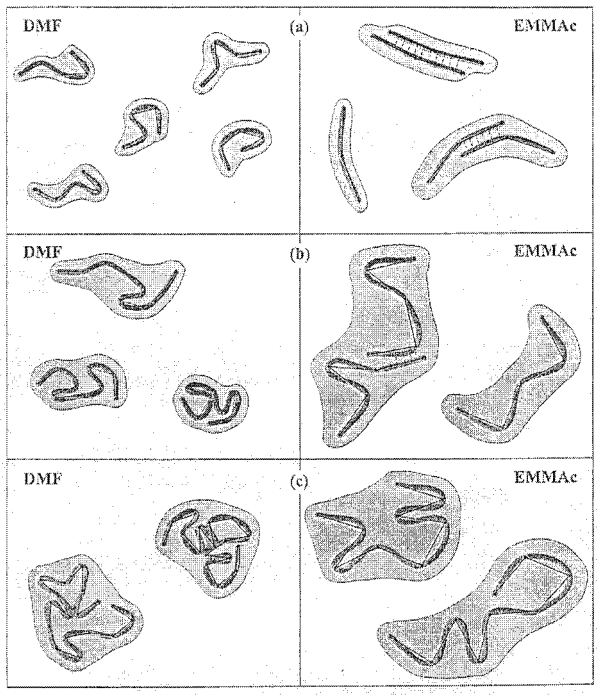

Fig. 46 Schematic representation of cellulose derivatives of various chain lengths monodispersely dissolved in dilute solutions of DMF (N,N-dimethyl formamide) and EMMAc (2-methoxyethyleneacetate); number of chains and contour length are the same comparing equal molecular mass in both solvents but the Kuhn segment length l_k are different: $2l_k(DMF) = l_k(EMMAc)$ (experimental value); number of Kuhn segments N_k are increasing from (a) to (c): (a) $N_k(DMF) = 4$, $N_k(EMMAc) = 2$; (b) 8 and 4, (c) 16 and 8, respectively. The worm-like chain is represented by broad dark lines, Kuhn segments by thin lines, and the shadows show the overall shape of the molecules with solvent attached (from [77]).

These findings demonstrate the dominating role of solubility in producing and processing of 2.5 acetate. It is conceivable that acetylation of cellulose to CTA will not completely break up the original fringed micelles of cellulose and that some hydrogen-bonded parts are still present forming the core of non-soluble domains. On the other hand crystalline domains of trisubstituted cellulose may hinder deacetylation of the almost fully acetylated product to 2.5 acetate. These

domains will not be soluble in acetone forming aggregates. Blocks of hydroxyl and trisubstituted acetyl groups may be situated along the chain forming non-soluble domains in acetone causing a strange solubility behavior of secondary cellulose acetate as discussed later.

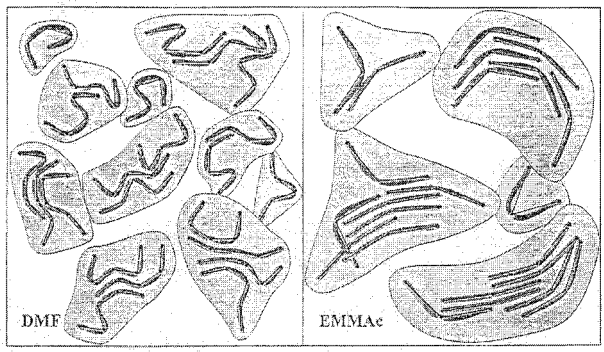

Fig. 47. Schematic representation of reversible associates of cellulose derivatives of low molecular mass in semi-dilute solutions. It should be noted that the contour length and the number of chains are the same in both drawings (solvents) (from [77]).

Increasing the concentration, coming to the semi-dilute solution, reversible association occurs forming structures as depicted in Fig. 47 for low molecular mass compounds and gels for high molecular mass compounds. These associates have to be considered the basic building blocks for the liquid crystalline state, which will be formed by further increased concentration. A more detailed investigation has shown that the size of the associates of cellulose derivatives in DMF solutions is smaller with smaller number of molecules involved as compared to associates in EMMAc.

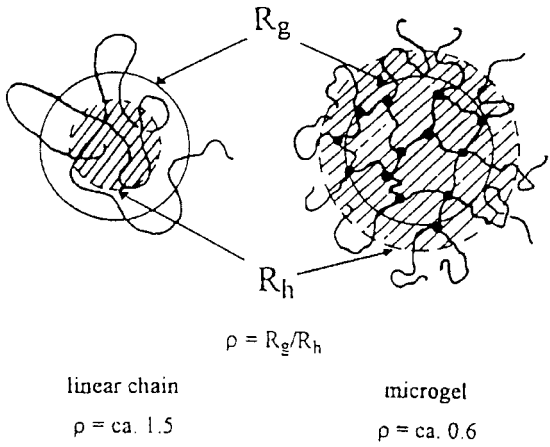

Fig. 48. Schematic representation of the radius of gyration R_g and hydrodynamic radius R_h of a linear chain and a microgel with the same R_g (from [81]).

Hydrogen bonds or strong polar interactions as well as hydrophobic interactions cause aggregation already in dilute solution, if the solubility parameters of solute or domains formed by blocks of chains and solvent disagree. These aggregates can be detected by static and dynamic light scattering and have been extensively discussed [78-81]. With static light scattering the radius of gyration R_g and with dynamic light scattering the hydrodynamic radius R_h can be determined. The ratio $\rho = R_g/ R_h$ is a measure for the shape and topology of particles in solutions as lined out in Fig. 48. In addition the molar mass of the particles is also available by static light scattering. Knowing the true molecular mass by choosing a solvent with single dispersed molecules and performing a light scattering experiment, the number of chains in a particle of an aggregate can be calculated. In commercial secondary cellulose acetate, aggregates have been established with more than 15 acetate chains depending on conditions (Fig. 49). These aggregates will further assemble by increasing concentration to a network of reversible associates. Their rheological properties may lie between those of a microgel and an entanglement network.

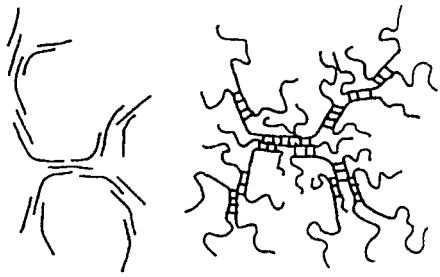

Fig. 49. Schematic representation of aggregated fringed micelles of commercial secondary CA. Simplified version (left) of the more realistic one (right; from [81]).

4.1.9 Commercial Secondary Cellulose Acetate in Solution

4.1.9.1 Multimodal Structures

A long time ago it has been recognized that secondary cellulose acetate produced from wood pulp had a higher viscosity then the one from cotton linters with similar characteristics [82]. This difference between viscosities for secondary CA processed from linters and that found from wood pulp is called false viscosity. The viscosity might also be affected by pretreatment and the kind of wood used. False viscosity is important in manufacturing acetate filaments, since it requires lower solution concentration of secondary CA from wood pulp for normal handling or it sacrifices yarn strength by going to a lower degree of polymerization. This effect was attributed to materials in cellulose such as pentosans and mannans as well as the orientation and aggregations of cellulose in the fibrils.

The availability of gel permeation chromatography (GPC), also termed size exclusion chromatography (SEC), helped to clarify some of the long known behavior of commercially produced cellulose acetate in solutions. A detailed investigation on commercial secondary CA from wood pulp with SEC led to a main peak as well as a prehump in elution chromatograms and only to a main peak for secondary CA from cotton linters [83]. This bimodal distribution of secondary CA processed from wood pulp indicates that at least two different kinds of structures are present in these secondary CA solutions. An analysis showed that the prehump in cellulose acetate (39-40% acetyl) in tetrahydrofuran was caused by hemicelluloses, and the kind of

acetylation also seemed to affect the prehump.

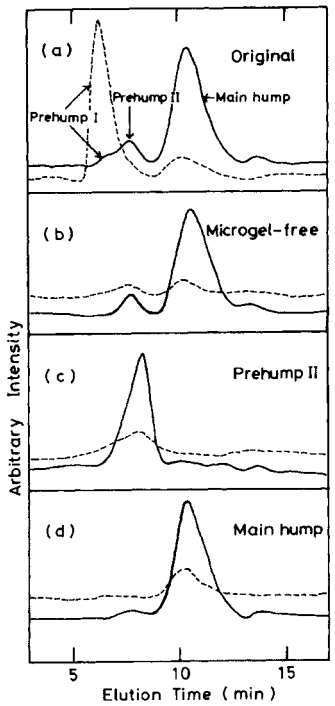

Fig. 50. GPC diagrams of original cellulose acetate (DS = 2.4) and its fractions in acetone solution. Detection by refractive index (RI) solid line, by light scattering (LS) dashed line (from [85]).

The characterization of secondary CA in acetone solutions, mostly used in processing, appears to be rather difficult for several reasons. Depending on the distribution of substituents on the anhydroglucopyranose unit and along the chains, the resulting different structural feature may affect the solubility. The solution properties may also be influenced by the residuals of the original pulp or linters and by the acetylation and partial deacetylation processes [84].

In Fig. 50 a gel permeation chromatogram (GPC) is presented, which suggests that several structural features in acetone solutions are present and have to be discussed for commercial CA (DS = 2.4) products even after filtration [85]. The original GPC diagram Fig. 50(a) shows several

peaks originating from pure secondary CA in solution (main hump and prehumps). Fig. 50(b) represents a microgel free fraction, which has been obtained by ultracentrifugation in acetone and Fig. 50(c) and (d) one or more fractions consisting of various aggregation or association of molecules, which can be separated by fractionation in a GPC column as depicted in (c) and (d). The large increase in the first peak, termed prehump I, by changing the detection from a refractive index detector (RI) to a light scattering detector (LS, LALLS) can be explained by compact, large particles, microgels, with a high molecular weight as suggested by the small elution time.

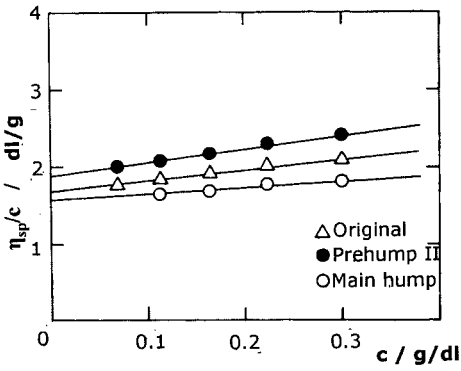

Fig. 51. Concentration dependence of reduced viscosity of the original CA (DS = 2.4) and its fractions in acetone (from [85]).

Table 8. Chemical composition, intrinsic viscosity [η], and number-average molecular weight M_n of original cellulose acetate and its fractions [85].

	Chemical composition (wt %)				
sample	glucose	xylose	mannose	[η] (dl g^{-1})	$M_n/10^4$ (D)
original	99	0.3	0.5	1.7	5.6
prehump 1	87	7	7	-	-
prehump 11	99.6	0.2	0.2	1.9	6.4
main hump	100	0	0	1.6	5.2

It is clear that the influence of such a secondary CA/ acetone solution on viscosity strongly depends on the presence and the size as well as the structures of the various fractions in this solution. The reduced viscosities η_{sp}/c as a function of concentration of secondary CA samples depicted in Fig. 50 are represented in Fig. 51 and lead to the conclusion that the true intrinsic

viscosity ($c \rightarrow 0$) of secondary CA can only be obtained after fractionation and removal of the disturbing structures. Table 8 lists the intrinsic viscosities of the fractions and the analysis of the chemical composition broken up in various sugar residues.

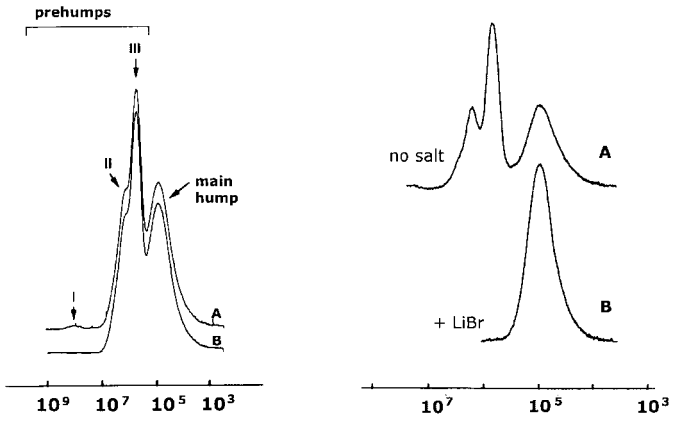

Fig. 52. SEC of secondary CA from Floranier pulp in DMAc. Abscissa calibrated by molecular weights of polystyrene standards; **(a)** curve A before and B after ultracentrifugation; **(b)** curve A correspond to curve B in Fig. 52a and B after addition of LiBr to the solution (from [86]).

Table 9. Chemical composition of microgel fractions in secondary CA solutions in acetone [86].

Compounds	sugar in secondary CA microgel from Floranier pulp (mol %)	sugar in secondary CA microgel from cotton linters (mol %)
xylose	30.6	8
mannose	10	4
glucose	56.4	87
galactose	0.4	-
uronic acids	2.6	1

A more detailed characterization of secondary CA from two sources, cotton linters and wood pulp from softwood, led to further clarification of the structural entities present in solutions [86]. Fig. 52 shows the size exclusion chromatograms (SEC) of secondary CA from Floranier pulp in DMAc after filtration (0.2 μm pore size) before and after ultracentrifugation. The microgel fraction

(prehump I) disappears after ultracentrifugation (cf. curve B in Fig. 52a). This microgel fraction consists of elongated narrow particles of 30-40 nm in length and 5-10 nm in thickness for secondary CA from cotton and of small shapeless aggregates either isolated or connected for secondary CA from Floranier pulp as represented in Fig. 53. The microgel composition of sugars is collected in Table 9. The ratio of the insoluble fractions of secondary CA amounts to more than 2:1 comparing Floranier pulp with cotton linters. From Table 9 it can be deduced that these microgels correspond to acetylated polysaccharides, xylan, mannan and cellulose, in different amounts for these two samples. Evaluation of the solubility in two solvents (cf. Table 10) led to further insights: the insoluble fraction in chloroform/ ethanol (9:1 vol%) contains a high percentage of xylose moieties for Floranier pulp as origin and consists entirely of glucose residues for cotton linters as origin. The soluble fraction has been attributed to xylan diacetate (XDA).

Table 10. Percentage and chemical composition of microgel fractions of secondary CA in acetone after redispersion in chloroform or a mixture of chloroform and ethanol (9: 1). A: soluble in $CHCl_3$, B: soluble in $CHC1_3$/ C_2H_5OH (9: 1), C: insoluble in $CHC1_3$/ C_2H_5OH (9: 1).

	Secondary CA microgel from Floranier pulp			Secondary CA microgel from cotton linters		
	A	B	C	A	B	C
wt%	13	74	13	25	60	15
mol %						
xylose	3	18	84	2	5	10
mannose	24	7	-	-	7	-
glucose	73	75	16	98	88	90

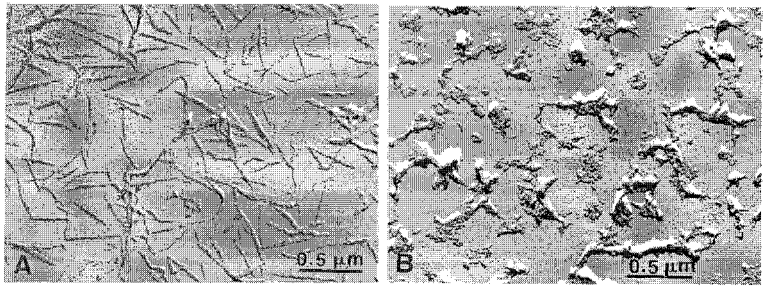

Fig. 53. Electron micrograph of microgel fragments occurring in secondary CA solution after drying. A: origin cotton linters, B: origin Floranier pulp (from [86]).

Further information on the microgel fractions of the two samples is provided by X-ray diffraction on the dried and annealed materials (Fig. 54). The Debye-Scherrer pattern of the microgel (part A), origin cotton linters, in Fig. 54a matches the diagram from a standard CTA II sample (part B). The X-ray diagram of the microgel (A), origin Floranier pulp, in Fig. 54b matches the xylan diacetate XDA (C) and the CTA II (B) standard. But it can be recognized that the intensities of the first two rings in the CTA II standard and the sample are quite different suggesting an overlap of CTA II and CTA I. The second ring is absent for CTA I but the first and the third ring, assigned to CTA I, have almost the same position as CTA II. Therefore, an overlap of CTA I and CTA II seems to be most probable and agrees with the findings of Ueda et al. [87] who proposed the existence of CTA I in microgels of secondary CA from wood pulp. The analysis of the X-ray study indicates that cellulose triacetate and xylan diacetate are present in the partial saponified materials, CTA I from heterogeneous, CTA II from homogeneous acetylation, and these products cannot be dissolved in acetone or DMAc.

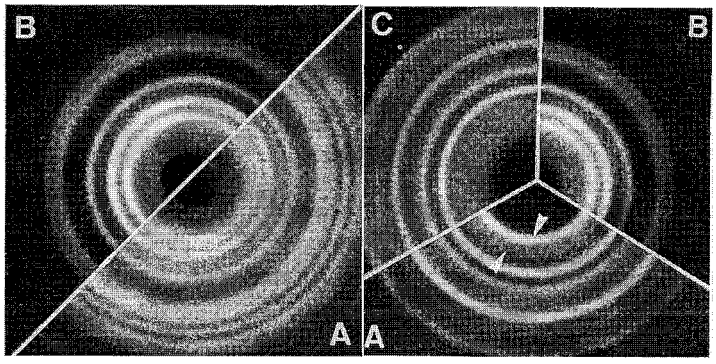

a **b**

Fig. 54. Comparison of Debeye-Scherrer X-ray diagrams of the microgel fractions of origin cotton (a) and origin Floranier pulp (b) with standards. The microgel fractions are termed A and corresponding standards: B for CTA II and C for XDA (from [86]).

Ionic effects cause the remaining prehumps II and III in the original SEC diagram. A complete carbanilation of samples, which should bring materials with free hydroxyl into solution, did not affect the appearance of the two peaks. But adding LiBr to the solution led to the disappearance of the prehumps as demonstrated in Fig. 52b. Further investigations confirmed that the extra

peaks correlate with ionic effects caused by the sulfate groups from the catalyst remaining and relate to the amount of residual calcium. Intermolecular ionic cross-linking between the sulfate groups and the divalent ions increases the molecular weight. A linear relationship has been established between the size (area) of the prehumps in the elution diagrams and the residual sulfur of the samples and presented in Fig. 55.

Multiple peaks in SEC of ionic polymers are often observed and the shifting or disappearance of peaks by adding a small amount of LiBr is well known. LiBr in DMAc and acetone breaks up the true ionic cross-linking of the sulfates and Ca ions that are capable of forming aggregates.

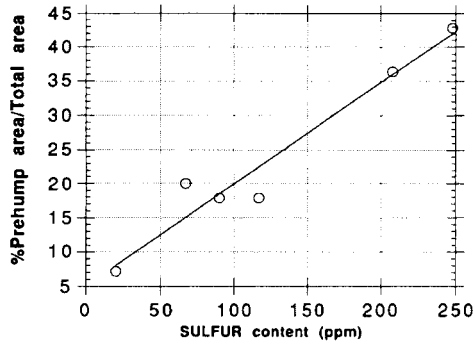

Fig. 55. Percentage of prehump area of SEC diagrams of secondary CA in DMAc from Floranier pulp as a function of residual sulfur after removal of the microgel fraction (from [86]).

4.1.9.2 Comparison of Commercial Samples of Different Origin

A characterization has been undertaken of commercial secondary CA of different origin and from various processes with the goal to clarify the polydispersity, the state of solution and aggregation in acetone. Some representative samples have been selected and the GPC diagrams are depicted in Fig. 56 [88]. The separation of the secondary CA samples into the various fractions was performed with appropriate gel permeation chromatography (GPC) with divinylbenzene/ styrene beads and three detector devices, laser light scattering (LALLS) detector at two angles 15° and 90°, refractive index (RI) and viscosity detector. The main fractions of all the materials investigated in GPC experiments exhibit similar molecular weights (main hump), but large differences have been detected in content, composition and structure of the microgels (prehumps), which consist of more or less aggregated CAc of normal chain length with deviations in the acetyl

number and with increased content of sulfur, calcium and hemicelluloses. The mass ratio of microgel to secondary CA varies considerably from 2 to 40%. The specific viscosity η_{sp} may be considerably influenced by the microgel fractions up to 60%. The microgels of the first fraction (prehump I) represent compact gels of size 0.15-0.45 μm causing a small viscosity signal as compared to the RI and LALLS signals and consist of increased content of hemicelluloses, sulfate as well as calcium. NMR investigations on prehump I detect predominantly low mobile CAc, mostly CA (DS ~2.5) and suggest an irregular distribution of DS along the CAc chain. A low viscosity contribution is found as compared to its concentration and supports the idea of compact particles with little bound solvent.

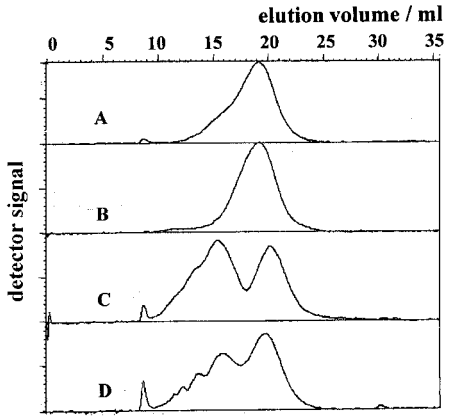

Fig. 56. GPC diagrams recorded with viscosity detector of selected commercial CA (DS ~2.5) of various origin (from [88]).

The second fraction (up to 5 peaks) consists of loose gels with 0.08-0.30 μm of size and exhibits high viscosity with regard to concentration. Further findings include weak cross-linking with bound acetone and a high content of xylan, mannan, sulfate and calcium. The gel can be dissolved by silylation/ acetylation in parts. A DS of ~2.5 is confirmed by NMR measurements with some deviation of a statistical distribution. High segmental motion confirms the model of a weakly cross-linked structure with bound acetone, which might occur in several aggregation states (several prehumps). The aging and stability are different for these CAc, and the aging effect

increases with higher content of loose gels and free acid.

The main fraction or main hump consists of CA (DS ~2.5) to more than 99% with statistical acetyl distribution as determined by NMR and confirmed by IR. The chain segments are mobile, and the main hump contains very low amounts of sulfate and calcium as well as xylan and mannan. The distribution of CA (DS ~2.5) molar mass ranges from $20 \cdot 10^3$ to $250 \cdot 10^3$ D (polystyrene equivalent). Because of the different sensitivity of the detector systems for various uniform molar masses, the maxima of GPC curves may be shifted to some extent for different detection methods employed. Sometimes so-called posthumps are observed which consist of low molecular weight compounds as decomposition products of CAc, acetic acid etc.

A fractionation with acetone/ cyclohexane led to enriched and isolated microgels, which exhibit normal acetyl numbers of 54-56. However, an unusual distribution of acetyl groups along the chains may influence the solubility. An analysis of soluble secondary CA (main hump) and microgel (prehump) of the samples shown in Fig. 56 are listed in Table 11. The microgel fraction contains significant higher values in ions and xylan.

Table 11. Amount of ions and hemicelluloses of the main hump and prehumps as well as of the sol and gel fractions of secondary CA samples presented in Fig. 56 (from [88]).

		Main hump[1]	prehump[2]	in solution	precipitate	in solution	precipitate
sample		B	D	A	A	C	C
Ca^{++}	/ ppm	39.5	230.8	38	126.8	189.4	441.5
Na^{+}	/ ppm	109.5	267.9	73.6	394.4	85.3	163.4
Mg^{++}	/ ppm	3,1	12.6	8.4	0.4	2.9	18.4
SO_4^{--}	/ ppm	51.8	482.2	172.9	1922.1	399.1	695.2
xylan	/ %	0.34	1.77	0.45	2.63	0.58	2.60
mannan	/ %	.0.32	10.51	10.28	1.32	0.23	0.82

[1] prehump free, [2] ca 85% prehump

In a first precipitation step at 80% acetone / 20% cyclohexane (41.6 mass%) an enriched microgel phase was obtained with a significant higher ion content in the sol fraction with the exception of Mg and mannan for sample A. The ratios of gel to sol fractions are smaller for sample C as compared to sample A (Table 11).

4.1.9.3 Comparison of Molecular Weights of Commercial Samples

It should be emphasized that molar mass determination by viscosimetry using the intrinsic viscosity [η] - molar mass M relationship may be strongly influenced by aggregation. This fact may have caused the many discussions about the constants in the [η] - M relationship for 2.5 cellulose acetate found in literature. An investigation on various molar mass samples ordered from a catalogue of one supplier was carried out, and the molar masses provided by the supplier are listed in Table 12. Included in this table are the elution volumes of the peaks of the main fractions of a GPC elution diagram (Fig. 57) representing the average molar mass [88]. The GPC data contradict the provided molar masses of the samples. The elution volumes of the peaks are the same within experimental error with the exception of sample A. This sample A contains a low sulfate value of 191 ppm as compared to 543 ppm for sample C and points to less cross-linking and less portions of prehumps with fewer sulfate groups.

Table 12. Characterization of secondary CA ordered from a commercial catalogue with the listed molecular weights and compared with the elution volume of the main peak of a GPC diagram (cf. Fig. 57; from [88]).

Sample		prehump I + II	main hump maximum (RI)
	M / D	/ mass %	elution volume/ ml
A	29.000	2	21.2
B	37.000	1	19.9
C	52.000	5	20.1
D	61.000	9	20.0

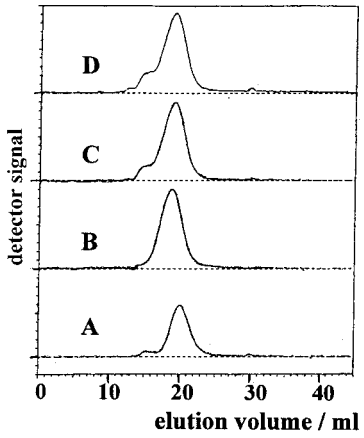

Fig. 57. GPC diagrams recorded with viscosity detector of selected CA (DS ~2.5) listed with various molecular weights in a catalogue (cf. Table 12; from [88]).

4.1.10 Solution and Flow Properties

The solubility of cellulose acetate depends on the average degree of substitution, the distribution of substituents along the chain and the distribution on the primary and secondary alcohol groups and will be addressed in details in Chapter 4.2. Correlations are discussed concerning the substitution pattern, which may be available by chemical or NMR methods. These structural characteristics affect the viscosity of solutions and compatibility with softeners, resin, varnish etc. The solubility properties of hydrolyzed commercial cellulose acetate are indicated in Table 13, and in Table 4 of Section 4.1.3 some details are provided about the distribution of substituents during saponification in different media. The also important resistance to chemicals and solvents is summarized in Chapter 5.3, Table 9.

Table 13. Solubility of commercial cellulose acetate in various solvents (from [75]).

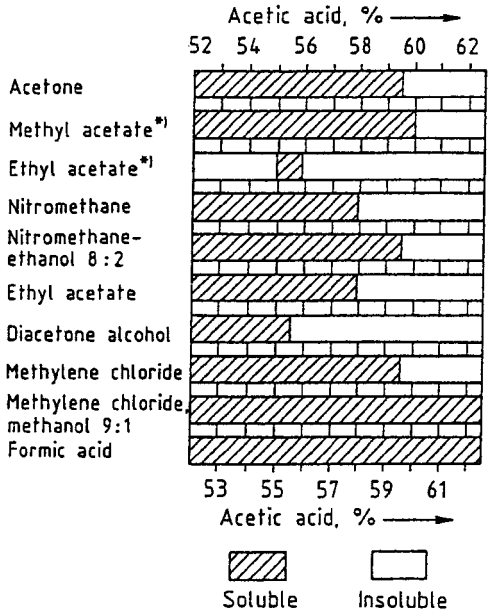

*Technical grade

4.1.10.1 Dilute Solutions – Intrinsic Viscosity

Molecular properties as molecular mass, the state of solution and geometric extension of the macromolecules are available by careful evaluations of dilute solutions. Viscosity measurements represent a simple experimental method for molecular mass determination. Further methods as osmometry, sedimentation in the ultracentrifuge, light scattering and their limitations can be found in textbooks. The intrinsic viscosity [η], which is related to molar mass by equation (1), will be obtained by extrapolation of the reduced viscosity η_{sp}/c to concentration $c \rightarrow 0$ and shear rate $d\gamma/dt \rightarrow 0$. The so-called viscosity-average molecular mass M_v determined by this method lies between the mass-average M_w and the number-average M_n that are available by light scattering and osmometry, respectively, and the special relationship $M_v = M_w$ holds for **a** = 1. For **a** close to 1, the mass-average M_w represents a good approximation. However, it should be emphasized that in case of molecular mass distribution functions with constant ratios of M_v/M_n and M_v/M_w independent of molecular mass as in the normal Schulz-Flory distribution function,

the relationship of eq. (1) holds for $M = M_w$ and $M = M_n$ but with different constants K_m in these two cases. If the calibration for the constants K_m and **a** is carried out with samples following the above mentioned molar mass distribution, the intrinsic viscosity can be used to determine M_w and M_n.

Since osmometry has been the method of choice to determine molar masses for a long time, the number-average molar mass M_n was used for calibration proposes by eq. (1). When light scattering techniques became available in the 1940th, this method was preferred and M_w used to overcome the limitations of osmometry. The molar mass can be determined by eq. (1), if the appropriate constants are known, which have been carefully evaluated by many investigations. Commercial secondary CA normally shows multimodal distribution, the knowledge of which is a necessity for an evaluation of intrinsic viscosity, and therefore, a number of different values for K_m and **a** have been published and discussed in the literature. A detailed discussion started after the introduction of GPC chromatography, and the various averages of the molecular mass distribution could be evaluated and tested.

The calibration parameters K_m and **a** have been carefully determined for CAc fractions of solutions with low polydispersity of M_w/ M_n of 1.2-1.4. Care was taken during the derivatization reactions that only a single peak appeared in GPC diagrams (uni-modal distribution) and light scattering experiments suggested a molecularly dispersed system [89]. The mass-average M_w was determined by light scattering and M_n by osmometry. The values for M_w, preferred for calibration, K_m and the constant **a** are listed in Table 14 for various DS and solvents with details on the substitution patterns at the anhydroglucopyranose unit. The constant **a** is < 0.8 as for most synthetic polymers and exceeds 0.8 occasionally, if the number average molecular mass M_n is used and if samples possess too broad polydispersity (M_w/M_n).

Table 14. K_m and exponent **a** in the intrinsic-molecular weight (M_w) equation ($[\eta] = K_m M_w^a$) for various cellulose acetate CAc at 25 °C and degree of substitution at various positions by ^{1}H- and ^{13}C-NMR determined in deuterated solvents [89].

DS of CAc	solvent	$K_m x 10^2$ [cm^3/ g]	**a**	position	^{1}H-NMR	^{13}C-NMR
2.92	TFA[a]	3.96	0.70_6			
	DMAc[b]	2.64	0.75			
	acetone	2.89	0.75_5			
	TCM[c]	4.54	0.64_9	C6	0.99	1.00
				C2	1.01	1.02
				C3	1.092	0.89
	DCM[d]	2.47	0.70_4			
2.46	DMAc[b]	1.34	0.82			
	acetone	13.3	0.616	C6		0.82
				C2		0.75
				C3		0.89
	THF[e]	5.13	0.68_8			
1.75	DMAc[b]	9.58	0.65			
	DMSO[f]			C6		0.59
				C2		0.53
				C3		0.63
0.49	formamide	20.9	0.60			
	water	20.9	0.60			
	DMSO[f]	17.1	0.61	C6		0.19
				C2		0.10
				C3		0.20
	DMAc[b]	19.1	0.60			

[a] trifluoroacetic acid; [b] N,N-dimethylacetamide; [c] trichloromethane; [d] dichloromethane; [e] tetrahydrofurane; [f] dimethylsulfoxide

Numerous values for the adjustable parameters **a** and K_m for secondary CA in a single solvent acetone have been proposed regarding eq. (1). These parameters depend as shown in Table 14 besides on the solvent system, on the degree of substitution but also on temperature and are only valid in a specified molar mass range. For CA (DS =2.46) in acetone or in THF this range extends from 60 $10^3 < M_w < 260\ 10^3$ D concerning **a** and K_m as provided in Table 14. Almost all authors who have investigated secondary CA used commercial products, which in most cases exhibit multi-modal molecular mass distributions and were not carefully characterized as well as eq. (1) often calibrated against M_n from osmometry, at least in older publications. The values for **a** range from $0.67 < \mathbf{a} < 1.0$ and are only valid for the specific samples used. As expressed by Kamide et al. [90] this wide variation on **a** and also on K_m can be reasonable explained by polydispersity

effects of the samples, since **a** increases with polydispersity. Nevertheless, two extensive studies should be addressed [19, 91]. In 1951 the equation

$$[\eta]\ (25\ ^{\circ}C,\ \text{acetone}) = 8.97\ 10^{-5}\ M_n^{0.90}\ (\text{unit of } [\eta]\ 100\text{ml/g}) \qquad (4)$$

was published after an investigation of 14 fractions of secondary CA by repeated refractionation and for molecular masses up to $115x10^3$ D. A similar large value **a** = 0.818 was obtained for CA (DS =2.45) in THF [91].

If the value for **a** in Table 14 for CA (DS =2.46) in acetone is calculated for M_n as variable in eq. (1) **a** = 0.643 is obtained attributed to the narrow polydispersity. For a monodisperse sample the parameters are **a** = 0.616 and $K_m = 0.136\ cm^3/g$. at 25 °C, which is very close to the values listed in Table 14. The theoretical value for **a** in good solvents amounts to 0.764 following the scaling laws [81].

Table 15. Number-average molecular mass M_n of cellulose acetate fractions with DS = 2.46 in tetrahydrofuran THF determined by various methods as MO, GPC and VPO (in $M_n x10^{-4}$ /D); M_w was received by light scattering (from [89]).

Sample		MO	GPC	VPO	M_w/M_n
CA(2.46)	1	2.7	4.1	2.6	1.66
	2	4.8	5.0	4.1	1.59
	3	5.5	5.8	5.4	1.36
	4	8.7	8.8	8.1	1.25
	5	12.2	11.9	11.1	1.25
	6	12.6	12.3	12.9	1.28

The temperature dependence of the intrinsic viscosity of secondary CA is in sharp contrast to the findings of vinyl polymers exhibiting a negative temperature gradient for secondary CA (Fig. 58) and has been explained by a rapid decrease in the unperturbed chain dimension with increasing temperature as the dominant effect.

Studies of colligative properties of solutions as the vapor pressure (VPO) for small molar masses or osmotic pressure (MO) result in the determination of the number-averaged molar mass M_n. This quantity can also be obtained from gel permeation chromatography. The values obtained for various M_n of secondary CA samples are compared in Table 15 and lead to the conclusion of molecularly dispersed structures in solution for these compounds.

Changes in M_n may occur due to aggregation and have been actually observed. M_n determined by membrane osmometry in tetrachloroethane (TCE) decreases with increasing temperature approaching M_n as determined by MO in THF. The CA (DS ~2.5) molecules have a considerable tendency to form aggregates in poor solvents as in TCE below 70 °C. Burchard et al. [78-81] have extensively investigated the aggregation of commercial 2.5 acetate in acetone by light scattering and developed models and proposed structural details of the aggregates.

Light scattering experiments are the method of choice for testing solutions for molecular disperse distributions and to study structural features as well as the molecular mass M_w. Besides these important properties to characterizing cellulose acetate solutions for application, several features are also available for proposing structural models as persistence length, radius of gyration, and by dynamic light scattering the hydrodynamic radius.

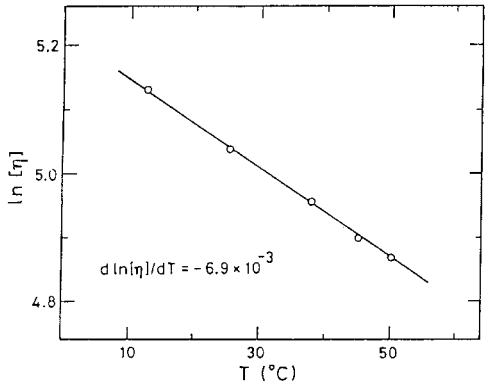

Fig. 58. Temperature gradient of intrinsic viscosity for secondary CA fraction in acetone (from [89]).

Careful fractionation and preparation of CA (DS =2.46) led to excellent agreement of the M_w values in good solvents and point with the interpretation of the resulting Zimm plots towards molecularly dispersed solutions for these secondary CA. A statically distribution of acetyl groups at the anhydroglucopyranose unit and along the chain may play a decisive role.

It should also be mentioned that CTA dissolves in acetone by a special treatment despite the fact that it has been termed non-soluble in acetone. If a slurry of CTA in acetone is cooled to –40 °C or below and then warmed up to room temperature, a very stable molecularly dispersed solution

is obtained [89].

4.1.10.2 Concentrated Solutions – Flow Behavior

In applications concentrated solutions of CTA or secondary CA have to be handled for economic reasons. The production of solid materials utilizing concentrated solutions e.g. membrane formation or spinnability of fibers is influenced by viscoelastic and rheological properties as well as heat and mass transfer rates. We will not discuss the technical and engineering problems involved rather will only address some basic properties of the flow behavior of concentrated solutions. Important progress in fundamental studies have been achieved in water soluble cellulose derivatives after appropriate investigation tools and materials characterizations have been accessible. The flow behavior has been related to molecular parameters as molar mass and molar mass distribution, substitution pattern and substitution distribution but also to structural properties as molecular conformation, interactions and supramolecular structures [92]. Such extensive investigations have not been carried out for CAc in solutions e.g. in acetone.

In an experimental study of rheological properties and spinnability [93], data that have been collected by an Instron capillary rheometer illustrating rheological properties of concentrated solutions at a temperature, which lies almost 10 degrees over the boiling point of acetone.. In Fig. 59 the viscous response to shear of variously concentrated solutions has been represented as a basic step to characterize the flow behavior. Polymers including secondary CA in solution exhibit a shear-rate dependent viscosity above a critical shear rate. This critical shear rate divides the flow curve in two sections: a range, in which the viscosity, termed zero-shear viscosity η_o, is independent of shear rate and a range, which for secondary CA can be described by a power law, and the flow behavior is called pseudo-plastic flow or shear-thinning. The maximum gradient of the flow curves is the same for all concentrations and in the case of water soluble cellulosics, the viscosity for different molar masses remains the same at constant concentration [92]. Further, the width of the transition range from zero-shear viscosity η_o to the power law region is mainly determined by the polydispersity of the cellulose derivatives. The cause of shear-thinning may be disentanglements of coils for high molecular weights or a breaking up of associations and increased orientation of molecular segments in flow direction.

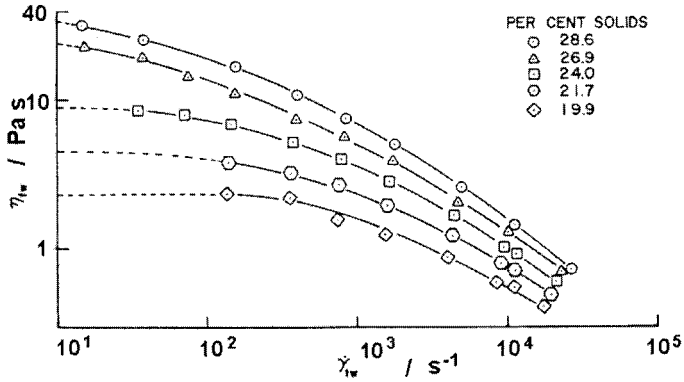

Fig. 59. True viscosity η_{tr} versus true shear rate $d\gamma_{tr}/dt$ for secondary CA/ acetone solutions for five concentrations with 5.8 mass-% water at 60 °C (from [93]).

Light scattering on concentrated CA (DS =2.43) in acetone shows conclusively that aggregation does take place leading to inhomogeneities [94]. It has been speculated that the small-angle X-ray scattering is caused by heterogeneities associated with poorly ordered regions with a correlation length of the order 35-50 Å. These heterogeneities are preserved, if films are prepared from concentrated solutions and extensive intermolecular association occurs. Increasing the concentration the poorly ordered regions rise to about 100-200 Å in diameter surrounded by much larger regions, non-uniform in polymer concentration. A densification seems rather difficult by solidification and a state created, which differs from the usual amorphous state. It has been speculated that these structural features make cellulose acetate a superior membrane for hyperfiltration applications. Cellulose acetate in films undergoes a thermal transition leading to enhanced mobility around 180 °C corresponding to a glass transition but still behaves like a vicoelastic solid with substantial intermolecular aggregations to temperatures as high as 210 °C. This behavior may cause the transitions and peaks in the thermograms and/or crystallization discussed in Section 4.1.4.1.

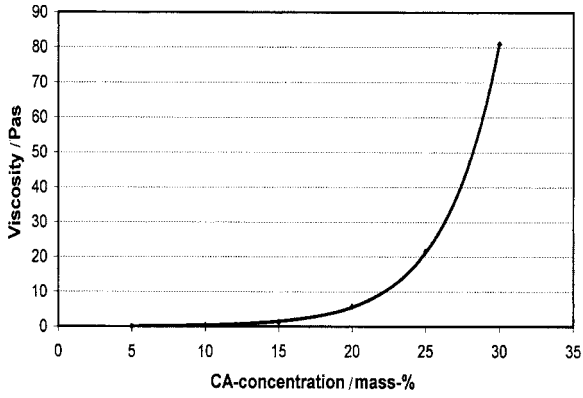

Fig. 60.Viscosity as a function of secondary CA-concentration at 40 °C and a shear rate of 1.2 s^{-1} (DP = 220, DS ~2.5; 3 mass-% water, 20 % microgel; from [95]). The curve can be represented by an exponential function.

The extrapolation of the flow curves in Fig 59 leads to the zero-shear viscosity η_o, which rises with concentration by an increase in segment density with concentration and also by molar mass and causes an increase in intermolecular interactions. A power law [93] has been presented for secondary CA with an exponent of 7.5 for the concentration range considered in Fig. 59. Describing the viscosity determined by an online capillary rheometer at low shear rate and avoiding the extrapolation leads to the curve represented in Fig. 60, which can excellently be fitted by a simple exponential function over the whole wide concentration range [95]. But this curve can also be divided into two power law functions from concentration ranges 5 to 18 and 18 to 30 mass-% CA (DS ~2.5). In the high concentration range the exponent almost reaches the stated value of 7.5. An interpretation of the mathematical functionality will depend on the effect of structural changes occurring during the rise of concentration. The onset of associations detected by light scattering for trisubstituted cellulose derivatives, but not for e.g. polystyrene, has been observed shortly above a critical concentrations described by (A_2M_wc) ~1-3 (A_2 second virial coefficient as interaction parameter) starting from a dilute particle solution into the semi-dilute solution range (cf. Section 4.1.8) [76, 77]. Structural changes have been proposed at still higher concentration leading to a further critical concentration but have not yet been studied. Also, for water soluble cellulose derivatives, a pronounced increase of zero-shear viscosity occurs

above a critical molar mass and/or concentration and has been shown to obey power laws below and above this critical point creating two ranges with different exponents [92].

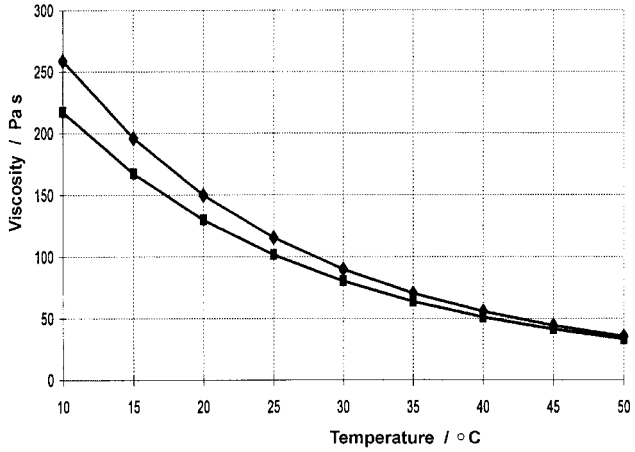

Fig. 61. Viscosity as a function of temperature for a secondary CA-concentration of 29.0 mass-% and 3 mass-% water (DP = 220, DS ~2.5; 20% microgel). Shear rate for upper curve 10 s^{-1}, lower curve 15 s^{-1} (from [95]).

The temperature dependence of the viscosity can be described with an Arrhenius equation, and the activation energy of the flow process has been determined from curves as depicted in Fig. 61. The activation energy decreases with increasing shear rate. A significant distinction of various commercial secondary CA qualities could not be established.

4.1.11 Lyotropic Liquid Crystals

In the last two decades optically anisotropic solutions of several cellulosic materials have been discovered and extensively investigated. Since anisotropic solutions for fiber spinning (dopes) of aromatic polyamides led to the production of aramid fibers of high tenacity and modulus as well as further unusual properties, the attention was focused to producing high performance cellulosic materials from anisotropic dope and also to investigate these materials from a basic scientific point of view.

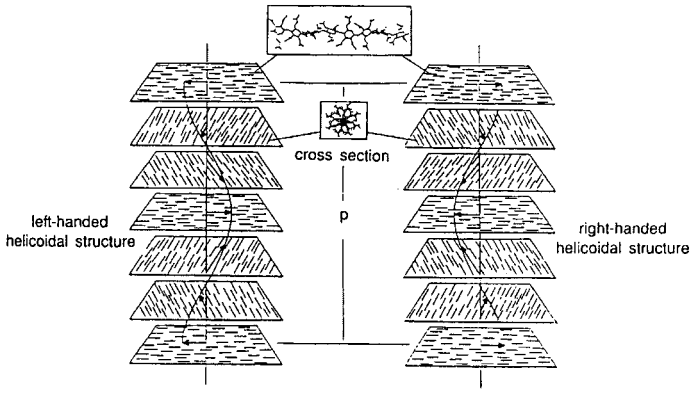

Fig. 62. Schematic representation of a helicoidal chiral nematic structure with pitch P. Right-handed twist: P>0; left-handed twist: P<0.

Anisotropic solutions are formed at high cellulosic concentrations of about >30 wt% and exhibit structures and properties, which will be presented in a short account. A more elaborate description will be found in overviews on this subject [1]. It should be emphasized that not all cellulosic solutions form anisotropic lyotropic phases at high concentrations and it is sometimes difficult to find suitable solvents for certain derivatives, including CAc [96, 97]. In general chiral nematic phases are formed, since the cellulose backbone exhibits a chiral nature, and the chirality is transmitted into the liquid crystalline state. In Fig. 62 the idealized structure of the chiral nematic state is represented, which consists of twisted nematic sheets with a repeat distance P, also called pitch. The inverse pitch P^{-1} is termed twisting power. This chiral nematic structure exists in small domains, which can be oriented by surface or flow effects, or these domains may be randomly distributed within the highly concentrated solution. The pitch is a quantity easily determined in experiments by several methods. (i) Direct methods as the Grandjean or Cano technique and by measuring the so-called fingerprints, dark and bright lines appearing by proper orientation of the domains. (ii) Chiral nematics exhibit selective reflections when viewed along the helicoidal axis, and the color appearing is related to the pitch by $P = \lambda_o / n$, λ_o the wavelength of the reflective color and n the average refractive index of a nematic sheet. The pitch is an important property considering optics and depends on external variables as temperature,

concentration and internal variables as substituents at the cellulose backbone and their distribution, degree of polymerization etc. Theoretical consideration for the pitch have not led to an acceptable agreement with experiments, probably because molecular dispersed structures were assumed in solutions but in reality reversible associates are present already in the semi-dilute state and will certainly be present in highly concentrated solutions. However, the pitch is less important considering the rheological properties, in particular the viscosimetric behavior, which is crucial for the spinning process. As proposed by Onogi and Asada [98] by rheo-optical experiments the shear rate dependence of the viscosity consists of three regions depicted in Fig. 63.

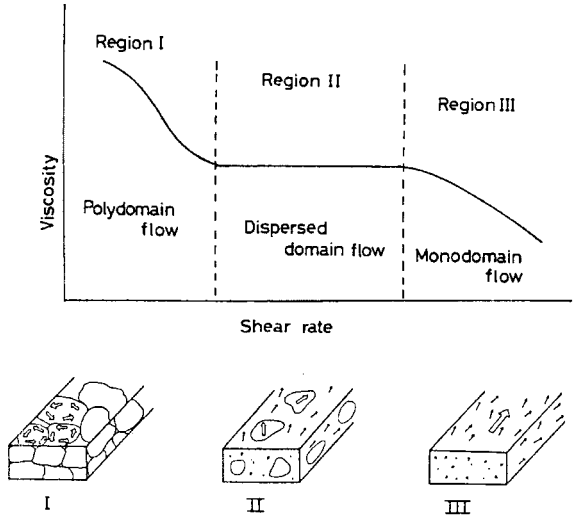

Fig. 63. Schematic flow curve of liquid crystalline cellulose derivatives (from [99]) and representation of the models for region I – III (from [98]).

A polydomain flow moves to a monodomain one through a dispersed domain flow that is from region I to region III (cf. Fig. 63 lower part). Sometimes region II may be missing. The solution in the isotropic phase does not exhibit region I. If the viscosity is plotted versus concentration, a steep decrease in viscosity is observed when the solution passes from the isotropic to the anisotropic phase through a biphasic region as shown in Fig. 64a and rises again at a lower level

in the anisotropic phase [99]. The onset of concentration into the biphasic region c_a and into the isotropic region c_b is marked in this figure. Likewise, a jump of viscosity occurs passing from the anisotropic into the isotropic region by increasing the temperature at constant concentration, and the extreme values of the curve are marked as T_{min} and T_{max} in Fig. 64b representing the width of the biphasic region.

Investigations were performed on liquid crystalline solutions of cellulose triacetate in trifluoroacetic acid (TFA), dichloroacetic acid (DCA) and mixtures of trifluoroacetic acid with halogenated solvents (CH_2Cl_2, 1,2-dichloroethane (1,2-DCE) and $CHCl_3$) [96]. The effect of solvent composition, temperature, polymer concentration, time, and a magnetic field on the pitch

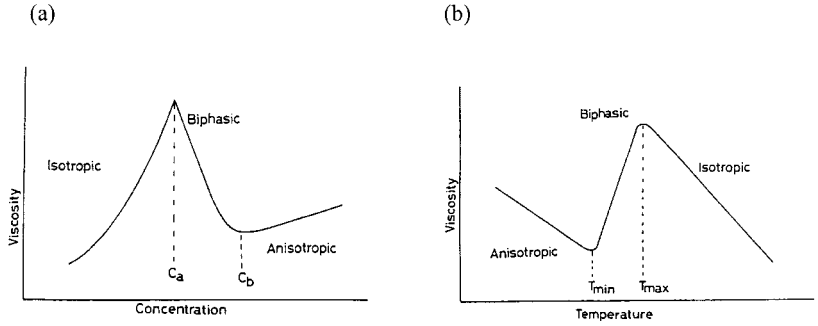

Fig. 64. Schematic dependence of viscosity (a) on concentration and (b) on temperature for lyotropic liquid crystals (from [99]).

of the chiral nematic structure and the flow properties of solutions of CTA have been reported in various TFA-CH_2Cl_2 mixtures at constant volume fraction of CTA. It was concluded that the stronger the acid the lower the polymer concentration for the onset of the anisotropic phase, which is also true for CA (DS=2.45) [97].

$$TFA\text{-}CH_2Cl_2 > TFA\text{-}1,2\text{-}DCE > TFA > TFA\text{-}CHCl_3$$

TFA forms a dimer in 1,2-DCE, which is a stronger acid than monomeric TFA, and this is probably the reason for the mixture to be an excellent solvent for CTA. TFA does not interact with $CHCl_3$ and therefore, this mixture is a poorer solvent.

A study of anisotropic solutions of commercial CTA and CA (DS ~2.4) in TFA came to

interesting conclusions [100]. An initial rapid increase in the left-handed pitch occurs for secondary CA but not for CTA that is due to fairly rapid esterification in TFA to produce a mixed cellulose ester. The presence of considerable trifluoroacetate groups on the cellulosic chains causes a reversal of the handedness of the chiral nematic helicoidal structure and strongly influences the concentration dependence of the pitch. The pitch of lc CTA also increases but slowly with time measured in days indicating an ester exchange reaction. The reaction on both CAc takes place predominantly at the C6 position as determined by NMR spectroscopy. Only minor scissions of the chains have been observed within a 2-3 day period. THF is thus a rather reactive solvent for functionalized cellulose acetates.

Mesophases of cellulose acetate with DS = 0.5-2.9 in inorganic solvent mixture of sulphuric acid (SA), poly(phosphoric acid) (PPA) and water (W) (1/8/1, w/w/w) are generated about a CAc concentration of 20 -30 wt% and cellulose itself also forms lyotropic liquid crystals depending on the degree of polymerization [97]. The total degree of substitution for CAc was estimated by ^{13}C NMR measurements and found almost the same for the three possible sites at C2, C3 and C6 for each of the sample investigated. It seems that molar mass of CAc does not affect the concentration of c_a and c_b i.e. the onset and the width of the biphasic region [101]. The left-handed pitch lies in the range of visible wavelength in contrast to the above mentioned system with THF-CH_2Cl_2 where the pitch is in the 10 μ range and the pitch increases with DS. The temperature and concentration dependence of the twisting power has been given by

$$1/P = a\,(1\text{-}T/T_N) \qquad (5) \qquad \text{and} \qquad 1/P = a'c_p^{\,3} + b \qquad (6)$$

T_N being the temperature for which P becomes infinite (quasi nematic phase), constant a is independent of temperature (ranging from 1.64 10^{-3} nm^{-1} for DS=0 to 0.77 10^{-3} nm^{-1} for DS=1.75 and T_N from 361 to 376 K for the mentioned DS range); c_p polymer concentration and a' and b constants independent of c_p. These equations are not universal valid for cellulose derivatives.

The use of lyotropic liquid crystalline cellulose triacetate (dope) for the production of high tenacity/ high modulus fibers is described in a European patent [102]. The as-spun cellulose triacetate fibers with at least 42.5% by weight acetyl groups exhibit a tenacity of at least 10 dN/tex, an orientation angle, arcing of reflections representing the degree of orientation, of 35 ° or less, a lateral crystallite size of at least 130 Å and an exotherm in the DSC scan between 190 and

240 °C. The average molar mass was characterized by the inherent viscosity higher than 5 dl/g in hexafluoroisopropanol at 30 °C. Heat treatment in steam under tension improved tenacity to 10.6 dN/tex, the modulus to 155 dN/tex and the orientation angle to 20 °. The fibers were obtained by air-gap spinning from an optically anisotropic solution of 30 to 42% by weight of cellulose triacetate and a solvent mixture 58 to 70% by weight of an organic acid, preferably trifluoroacetic acid (TFA/H_2O), but also mixtures TFA/CH_2CL_2 or TFA/HCOOH, into a bath of methanol. Saponification of the triacetate fiber and heat-treatment provided a regenerated cellulose yarn with tenacity of at least 12.4 dN/tex and modulus above 220 dN/tex. Using commercial CTA for preparation of regenerated cellulose fibers from lc solutions instead of the specially prepared high molecular weight materials as in the work of O'Brien still led to excellent but somewhat lower values of tenacity [103]. The conclusion was drawn in this study that the molar mass is the primary parameter influencing tenacity and modulus of highly oriented fibers.

Despite impressive mechanical properties, which show the potential of processing filaments from liquid crystalline solutions, yarn is not produced by this process, may be due to the non-attractive chemicals for an industrial plant. It should also be noted that the fibers exhibit the crystalline structure of CTA I (cf. also the discussion on polymorphism of CTA in this Chapter, Section 4.1.3.3).

[1] General:
E. Ott, H. M. Spurlin, M. W. Grafflin, Eds. „*Cellulose and Cellulose Derivatives*", 2nd ed., Interscience Publishers, New York, 1955.
N. M. Bikales, L. Segal, Eds., „*Cellulose and Cellulose Derivatives*", Wiley-Interscience, New York 1971.
K. H. Meyer, „*Natural and Synthetic High Polymers*", 2nd ed., Interscience Publishers, New York, 1950.
W. Gerhartz, Ed., „*Ullmann's Encyclopedia of Industrial Chemistry*", Vol. A 5, 5th ed., VCH, Weinheim 1986.
H. F. Mark, N. G. Gaylord, N. M. Bikales, Eds., „*Encyclopedia of Polymer Science and Technology*", Vol. 3, John Wiley & Sons, New York 1965.
G. Becker, D. Braun, Eds., „*Technische Thermoplaste*", Kunststoff-Handbuch, Vol. 3, Hanser, München 1992.
D. Klemm, B. Philipp, T. Heinze, U. Heinze, W. Wagenknecht, „*Comprehensive Cellulose Chemistry*", Wiley-VCH, Weinheim 1998.
H. Domininghaus, „*Die Kunststoffe und ihre Eigenschaften*", Springer-Verlag, Berlin 1998.
W. E. Morton, J. W. S. Hearle, „*Physical Properties of Textile Fibers*", The Textile Institute, Manchester, 1986.
H. D. Noether, Cellulose triacetate: A material for separating chiral isomers, in „*Cellulosics Polymers*", R. D. Gilbert, Ed., Hanser Publishers, Munich, **1994**, 217-231.
K. Kamide, H. Iijima, Recent advances in cellulose membranes, in „*Cellulosics Polymers*", R. D. Gilbert, Ed., Hanser Publishers, Munich, **1994**, 189-206.
K. J. Edgar, C. M. Buchanan, J. S. Debenham, P. A. Rundquist, B. D. Seiler, M. C. Shelton, D. Tindall, Advances in cellulose ester performances and application, *Prog. Polym. Sci.* **2001**, *26*, 1605-1688.
Liquid Crystals:
D. G. Gray, B. R. Harkness,. Chiral nematic mesophases of lyotropic and thermtropic cellulose derivatives, in

„*Liquid Crystalline and Mesomorphic Polymers*", V. P. Shibaev, L. Lam, Eds., Springer Verlag, New York, **1994**, 298.
R. D. Gilbert, Cellulose and Cellulose Derivatives as Liquid Crystals, in „*Agricultural and Synthetic Polymers*", J. E. Glass, G. Swift, Eds., ACS Symposium Series 433, American Chemical Society, Washington, DC, **1990**, 259.
J. X. Guo, D. G. Gray, Lyotropic Cellulosic Liquid Crystals, in „*Cellulosics Polymers*", R. D. Gilbert, Ed., Hanser Publishers, Munich, **1994**, 25-45.
P. Zugenmaier, Polymer Solvent Interaction, in Lyotropic Liquid Crystalline Cellulose Derivatives in „*Cellulosics Polymers*", R. D. Gilbert, Ed., Hanser Publishers, Munich, **1994**, 71-94.
P. Zugenmaier, Cellulosic Liquid Crystals, in „*Handbook of Liquid Crystals*", Vol. 3, D. Demus, J. Goodby., G. W. Gray, H.-W. Spiess, V. Vill, Eds., Wiley-VCH, Weinheim, **1998**, 453-482.
P. Zugenmaier, Supramolecular Structure of Polysaccharides, in „*Polysaccharides*", S. Dumitriu, Ed., Marcel Dekker, Inc., New York **1998**, 57-100.
[2] H. Staudinger, special reprint from *Cellulosechemie*, **1938**, *36*.
[3] P. Karrer, „*Polymere Kohlehydrate*", Leipzig, 1925; P. Karrer, C. Naegeli, *Helv. Chim. Acta*, **1921**, *4*, 169-173.
[4] K. Hess, G. Schulze, *Liebigs Ann. Chem.* **1926**, *448*, 99-120; K. Hess, K. Pichlmayr, *Liebigs Ann. Chem.* **1926**, *450*, 21-29; K. Hess, K. Friese, *Liebigs Ann. Chem.* **1926**, *450*, 40-58.
[5] M. Bergmann, *Collegium* 1926, P. 488; *Ber. Deutsch. Chem. Ges.* **1926**, *59*, 2973-2981.
[6] R. O. Herzog, *Ber. Deutsch. Chem. Ges.* **1925**, *58*, 1254-1262; R. O. Herzog, D. Krüger, *Kolloid-Z.* **1926**, *39*, 250-252.
[7] R. O .Herzog, H. Kudar, *Z. Phys. Chem.* A. **1934**, *167*, 343-353.
[8] H. Staudinger, *Ber. Deutsch. Chem. Ges.*. **1920**, *53*, 1073-1085; H. Staudinger, G. Fritschi, *Helv. Chim. Acta* **1922**, *5*, 785-806.
[9] H. Staudinger, M. Lüthy, *Helv. Chim. Acta* **1925**, *8*, 41-64, H. Staudinger, *Z. Angew. Chem.* **1929**, *42*, 37-40.
[10] H. Staudinger, H. Johner, R. Signer, G. Mie, J. Hengstenberg, *Naturwiss.* **1927**, *15*, 379; *Z. Phys. Chem.* **1927**, *126*, 425-448; H. Staudinger, R. Signer, *Z. Kristallogr.* **1929**, *70*, 193.
[11] O. L. Sponsler, W. Dore, *Colloid Symposium Monograph* **1926**, 174-265.
[12] W. N. Haworth, *J. Soc. Chem. Ind.* **1927**, 295-300; *Helv. Chim. Acta* **1928**, *11*, 534-548.
[13] K. H. Meyer, H. Mark, *Ber. Deutsch. Chem. Ges.*. **1928**, *61B*, 593-614.
[14] R. Willstätter, L. Zechmeister, *Ber. Deutsch. Chem. Ges.* **1929**, *62*, 722-725; L. Zechmeister, G. Toth, *Ber. Deutsch. Chem. Ges.* **1931**, *64B*, 854-870.
[15] K. Freudenberg, „*Tannin, Cellulose, Lignin*", Springer Verlag, Berlin, 1933.
[16] K. H. Meyer, *Z. Angew. Chem.* **1928**, *41*, 935-946; H. Mark, *Naturw.* **1928**, *16*, 892-900.
[17} H. Mark, *Z. Phys. Chem.* B. **1929**, *2*, 128; K. H. Meyer, H. Mark, *Ber. Deutsch. Chem. Ges.* **1931**, *64B*, 1999-2002.
[18] H. Staudinger, W. Heuer, *Ber. Deutsch. Chem. Ges.* **1930**, 63B, 222-234.
[19] H. J. Philipp, C. F. Bjork, *J. Polym. Sci.* **1951**, *6*, 383-396 and 549-562.
[20] D. Klemm, B. Philipp, T. Heinze, U. Heinze, W. Wagenknecht, „*Comprehensive Cellulose Chemistry*", Vol. 2, Wiley-VCH, Weinheim 1998.
[21] R. Chandrasekaran, Molecular Architecture of Polysaccharide Helices in Oriented Fibers, in „*Advances in Carbohydrate Chemistry and Biochemistry*", D. Horton, Ed., Academic Press, San Diego, 1997, 311-439.
[22] K. Hess, C. Trogus, *Z. Phys. Chem.* **1928**, *B 5*, 161-176.
[23] K. Hess, C. Trogus, *Z. Phys. Chem.* **1930**, *B 9*, 169-172.
[24] B. S. Sprague, J. L. Riley, H. D. Noether, *Text. Res. J.* **1958**, *28*, 275-287.
[25] M. Takai, K. Fukuda, M. Murata, J. Hayashi, in „*Wood and Cellulosics*", J. F. Kennedy, G. O. Phillips, P. A. Williams, Eds., Ellis Horwood, Chichester, 1987, 111-117.
[26] S. Watenabe, M. Takai, J. Hayashi, *J. Polym. Sci.* **1968**, *C23*, 825-835.
[27] A. Kuppel, H. Bittiger, E. Husemann, *Kolloid-Z. u. Z. Polymere* **1972**, *250*, 623-624.
[28] R. St. J. Manley, *J. Polym. Sci.* **1963**, *A 1*, 1875-1892.
[29] H. Kono, Y. Numata, N. Nagai, T. Erata, M. Takai, *J. Polym. Sci.* **1999**, *A 37*, 4100- 4107; D. L. VanderHart, J. A. Hyatt, R. H. Atalla, V. C. Tirumalai, *Macromolecules* **1996**, *29*, 730-739.
[30] H. Kono, T. Erata, M. Takai, *J. Am. Chem. Soc.* 2002, *124*, 7512-7518.
[31] A. Kuppel, E. Husemann, E. Seifert, P. Zugenmaier, *Kolloid-Z. u. Z. Polymere* **1973**, *251*, 432-433.
[32] R. M. Wolf, E. Francotte, L. Glasser, I. Simon, H. A. Scheraga, *Macromolecules* **1992**, *25*, 709-720.
[33] P. Zugenmaier, in „*Cellulose and Cellulose Derivatives*", J. P. Kennedy, G. O. Phillips, P. A. Williams, I.

Piculell, Eds., Woodhead Publishing Ltd., Cambridge 1995, 381-392; K. Riehl, Dissertation, TU Clausthal, D-38678 Clausthal-Zellerfeld 1992.
[34] E. J. Roche, J. P. O'Brien, S. A. Allen, *Polymer Comm.* **1986**, *27*, 138-140.
[35] A. J. Stipanovic, A. Sarko, *Polymer* **1978**, *19*, 3-8.
[36] E. J. Roche, J. P. O'Brien, Crystalline Polymorphism of Cellulose Triacetate Fibers Spun from Lyotropic Solutions, in *„Proceedings of the International Symposium of Fiber Science and Technology, ISF-85"*, Hakone, Japan 1985, PIII-12, P. 71.
[37] W. J. Dulmage, *J. Polym. Sci.* **1957**, *26*, 277-288.
[38] E. J. Roche, H. Chanzy, M. Boudeulle, R. H. Marchessault, P. R. Sundararajan, *Macromlecules* **1978**, *11*, 86-94.
[39] M. Wada, L. Heux, Structure of Cellulose Triacetate, in *„Preprints of ICC2002"*, Kyoto, Japan 2002, P1-31, P. 71.
[40] P. Zugenmaier, A. Kuppel, *Colloid & Polym. Sci.* **1986**, *264*, 231-235.
[41] A. Tappe, *Diplomarbeit*, Institut für Physikalische Chemie der TU Clausthal, D-38678 Clausthal-Zellerfeld 1999.
[42] F. Leung, H. D. Chanzy, S. Pérez, R. H. Marchessault, *Can. J. Chem.* **1976**, *54*, 1365-1371.
[43] D. L. Dorset, *„Structural Electron Crystallography"*, Plenum Press, New York, 1995.
[44] K. Kamide, M. Saito, *Polymer J.* **1985**, *17*, 919-928.
[45] A. Takahashi, T. Kawaharada, T. Kado, *Polymer J.* **1979**, *11*, 671-675.
[46] C. J. Malm, L. B. Genung, J. V. Fleckenstein, *Ind. Eng. Chem.* **1947**, *39*, 1499-1504.
[47] J. K. Gillham, *AICHE J.* **1974**, *20*, 1066-1079.
[48] J. Russell, R. G. van Kerpel, *J. Polym. Sci.* **1957**, *25*, 77-96.
[49] A. F. Klarman, A. V. Galanti, L. H. Sperling, *J. Polym. Sci. A-2* **1969**, *7*, 1513-1523.
[50] L.-G. Tang, D. N.-S. Hon, Y.-Q. Zhu, *J.M.S.-Pure Appl. Chem.* **1996**, *A33*, 203-208.
[51] V. J. McBrierty, C. M. Keely, F. M. Coyle, H. Xu, J. K. Vij, *Faraday Discuss.* **1996**, *108*, 255-268.
[52] P. Zugenmaier, *J. Appl. Polym. Sci. Appl. Polym. Symp.* **1983**, *37*, 223-238; Eggert, U., *Dissertation*, TU Clausthal, D-38678 Clausthal-Zellerfeld 1985.
[53] M. Scandola, G. Ceccorulli, *Polymer* **1985**, *26*, 1953-1957.
[54] M. Scandola, G. Ceccorulli, *Polymer* **1985**, *26*, 1958-1962.
[55] M. Pizzoli, M. Scandola, G. Ceccorulli, in "*Wood and Cellulosics*", J. F. Kennedy, G. O. Phillips, P. A: Williams, Eds., Ellis Horwood Ltd., Chichester 1987, 105-110.
[56] G. Ceccorulli, M. Pizzoli, M. Scandola, *Polymer Comm.* **1986**, *27*, 228-230.
[57] J. Einfeldt, D. Meißner, A. Kwasniewski, *Prog. Polym. Sci.* **2001**, *26*, 1419-1472.
[58] W. E. Morton, J. W. S. Hearle, *„Physical Properties of Textile Fibres"*, The Textile Institute of Manchester,, Manchester 1986.
[59] W. Kast, M. Meskat, O. Rosenberg, A. K. van der Vegt, in *„Die Physik der Hochpolymeren"*, IV. Band, H. A. Stuart, Ed., Springer-Verlag, Berlin 1956, 427-520.
[60] T. Alfrey, Jr., *„Mechanical Behavior of High Polymers"*, (High Polymers, Vol. VI), Interscience Publ. Inc., New York 1948.
[61] H. Wakeham, Mechanical Properties of Cellulose and Its Derivatives, in *„Cellulose and Cellulose Derivatives"*, E. Ott, H. M. Spurlin, M. W. Grafflin, Eds., Part III, 2nd ed., Interscience Publishers, New York 1955, 1247-1355.
[62] R. Meredith, *J. Text. Inst.*, **1945**, *36*, T107-130; T147-164.
[63] G. A. Serad, Cellulose Esters, Organic Fibers, in *„Polymers: Fibers and Textiles, A Compendium"* J. I. Kroschwitz, Ed., John Wiley & Sons, New York 1990, 55-81.
[64] R. W. Work, *Text. Res. J.*, **1946**, *19*, 381.
[65] G. Susich, *Text. Res. J.* **1953**, *23*, 545.
[66] J. C. Guthrie, *J. Text. Inst.* **1957**, *48*, T193-202.
[67] R. L. Steinberger, *Text. Res.*, **1936**, *6*, 267-269.
[68] H. Leaderman, *„Elastic and Creep Properties of Filamentous Materials and Other High Polymers"*, The Textile Foundation, Washington, DC, 1943.
[69] R. Meredith, *J. Text. Inst.* **1952**, *43*, P755-764.
[70] S. E. Sheppard, P. T. Newsome, *J. Phys. Chem.* **1935**, *39*, 143-152.
[71] G. C. Gibbons, *J. Text. Inst.* **1953**, *44*, 201-208.
[72] S. E. Sheppard, P. T. Newsome, *J. Phys. Chem.* **1932**, *36*, 2306-2318.
[73] F. Müller, Ch. Leuschke, Organische Cellulloseester – Thermoplastische Formmassen, in *„Kunststoff – Handbuch, Vol. 3/1: Technische Thermoplaste"*, G. W. Becker, D. Braun, Eds., Hanser München 1992, 396-457.

[74] A. Kamm, K. H. Schüller, Insulation, Electric, in *„Ullmann's Encyclopedia of Industrial Chemistry"*, Vol. 18, Wiley-VCH, Weinheim 2003, 223-269.
[75] K. Balser, T. Eicher, M. Wandel, H.-J. Astheimer, Cellulose Esters, in *"Ullmann's Encyclopedia of Industrial Chemistry"*, Vol. A5, VCH, Weinheim 1986, 419-459; & L. Hoppe, H. Steinmeier, Vol 6, Wiley-VCH, Weinheim 2003, 647-693.
[76] E.-A. Klohr, *Dissertation*, TU Clausthal, D-38678 Clausthal-Zellerfeld 1995.
[77] K. Schmidt, *Dissertation*, TU Clausthal, D-38678 Clausthal-Zellerfeld 1999.
[78] W. Burchard, L. Schulz, *Das Papier*, **1989**, *43*, 665-674.
[79] L. Schulz, W. Burchard, R. Dönges, Evidence of Supramolecular Structures of Cellulose Derivatives, in *„Cellulose Derivatives"*, T. J. Heinze, W. G. Glasser, Eds., ACS Symposium Series 688, American Chemical Society, Washington, DC, 1998, 218-238.
[80] W. Burchard, *TRIP* **1993**, *1*, 192-198.
[81] L. Schulz, B. Seeger, W. Burchard, *Macromol. Chem. Phys.* **2000**, *201*, 2008-2022.
[82] G. A. Richter, L. E. Herdle, *Ind. Eng. Chem.* **1957**, *49*, 1451-1452.
[83] H. K. Johnston, S. Sourirajan, *J. Appl. Polym. Sci.* **1973**, *17*, 3717-3726.
[84] K. Kamide, T. Terakawa, S. Manabe, *Sen'i Gakkaishi* **1974**, *30*, T464-T470.
[85] Y. Funaki, K. Ueda, S. Saka, S. Soejima, *J. Appl. Polm. Sci.* **1993**, *48*, 419-424.
[86] E. Fleury, J. Dubois, C. Léonard, J. P. Joseleau, H. Chanzy, *Cellulose* **1994**, *1*, 131-144.
[87] K. Ueda, S. Saka, Y. Funaki, S. Soejima, *Mokuzai Gakkaishi* **1988**, *34*, 346-353.
[88] A. Stein, Rhodia Acetow, Freiburg, private communication 1997.
[89] K. Kamide, M. Saito, Cellulose and Cellulose Derivatives: Recent Advances in Physical Chemistry, in *"Advances In Polymer Sciences"*, Vol. 83, Springer-Verlag, Berlin 1987, 1-56.
[90] K. Kamide, T. Terakawa, Y. Miyazaki, *Polymer J.* **1979**, *11*, 285-298.
[91] D. W. Tanner, G. C. Berry, *J. Polym. Sci. Polym. Phys. Ed.* **1974**, *12*, 941-975.
[92] C. Clasen, W.-M. Kulicke, *Prog. Polym. Sci.* **2001**, *26*, 1839-1919.
[93] P. D. Griswold, J. A. Cuculo, *J. Appl. Polym. Sci.* **1974**, *16*, 2887-2902.
[94] K. D. Goebel, G. C. Berry, D. W. Tanner, *J. Polym. Sci.: Polym. Phys. Ed.* **1979**, *17*, 917-937.
[95] W. Koppe, Rhodia Acetow, Freiburg, private communication 2001; T. Faisst, *Studienarbeit*, Institut für Mechanische Verfahrenstechnik und Mechanik der Universität Karlsruhe (TH), Karlsruhe 2001.
[96] D. L. Patel, R. D. Gilbert, *J. Polym Sci., Polym. Phys. Ed.* **1983**, *21*, 1079-1090.
[97] S. M. Aharoni, *Mol. Cryst. Liq. Cryst.* **1980**, 56, 237-241.
[98] S. Onogi, T. Asada, in *„Rheology"*, Vol. 1, G. Astarita, G. Marucci, L. Nicolais, Eds., Plenum, New York 1980, 127-147.
[99] S. Suto, Cellulose Derivatives as Liquid-Crystalline Phase, in *"Polysaccharides"*, S. Dumitriu, Ed., Marcel Dekker, Inc., New York 1998, 925-968.
[100] A. M. Ritcey, K. R. Holme, D. G. Gray, *Macromolecules* **1988**, *21*, 2914-2917.
[101] I. Miyamoto, T. Matsui, M. Saito, K. Kamide, *Polymer J.* **1996**, *28*, 937-941.
[102] EP 0 103 398 B1 (1989); du Pont de Nemours, E. I., and Co., USA; inv.: J. P. O'Brien.
[103] R. D. Gilbert, X. Hu, R. E. Fornes, *J. Appl. Polm. Sci.* **1995**, *58*, 1365-1370.
[104] H. Temming, H. Grunert, H. Huckfeldt, *„Temming-Linters"*, Peter Temming AG, Glückstadt 1972.

4.1.12 Appendix

A1

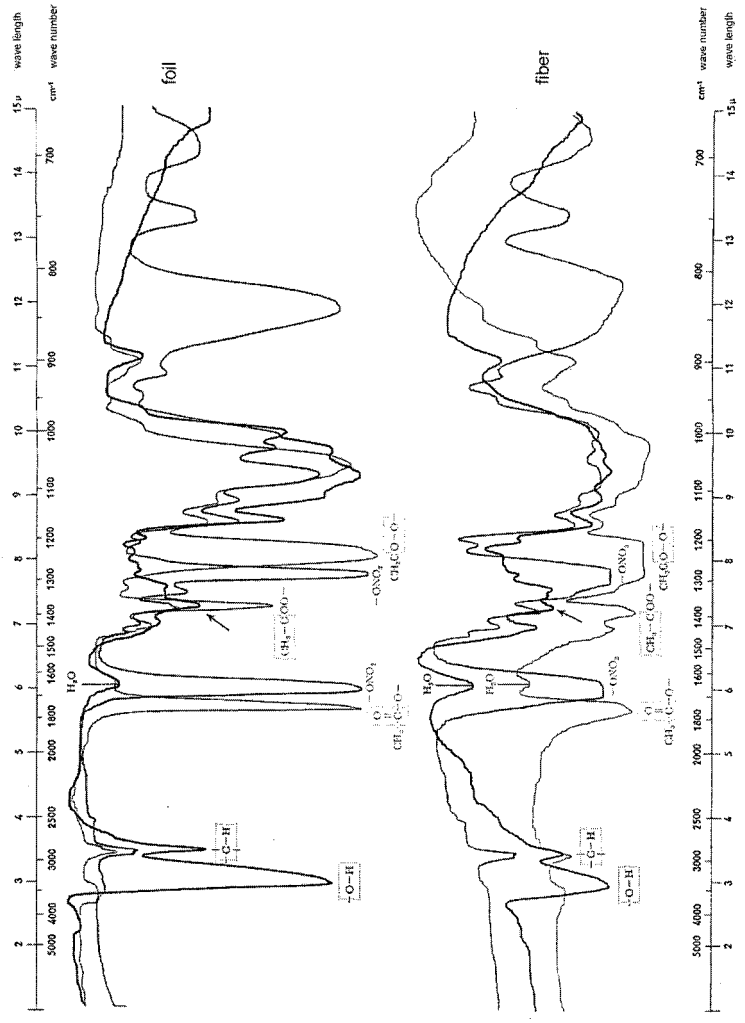

Fig. A1. IR spectra of cellulose, cellulose trinitrate (CTN) and cellulose triacetate (CTA) (from [104]).

A2

Conversion of units:

1 m = 39.4 in
1 kgf = 9.807 N
1 J = 0.24 cal
1 tex = 1 g/ km = 9 den
1 10^3 PSI = 6.9 MPa

1 kg = 2.2 lb
1 dyne = 10^{-5} N
1 Pa = 0.145 10^{-3} lbf / in = 0.102 10^{-6} kgf /mm^2
1 N/ tex = 102gf / tex = 11.3 gf / den
1 mil = 1 10^{-3} inch = 25.4 μm

The grex of a fiber, yarn, cord or rope is its fineness in grams per 10 km, the tex in grams per 1 km. 1 kgf or 1 gf represents the force of 1 kg or 1 g exerted in the gravitational field of the earth.
1 gf / grex = 1.11gf /den = 9.80 10^8 dyne/cm^2

The following relationship holds:

$$\sigma = f / \rho$$

stress f in N/ m^2, specific stress σ in N m/ kg, density ρ in kg/ m^3
or f in kN/ mm^2 (= GPa), σ in N/ tex and ρ in g/ cm^3
or f in N/ mm^2 (= MPa), σ in mN/ tex and ρ in g/ cm^3

A3

Data Sheet for Materials (from supplier)

Cellulose Acetate Sheet (Secondary CA)

		Conditions	ASTM
Mechanical Properties			
Tensile strength (MPa)	32-56	at break	D638
Flexural strength (MPa)	42-69	at yield or break	D790
Elongation (%)	20-50	at break	D638
Hardness	85-120	Rockwell R	D638
Izod impact (J/cm of notch)			
1/8 " thick specimen unless notched	1.1-4.5		D256A
Thermal Properties			
Thermal expansion coefficient (10^{-6}/°C)	100-150		D696
Thermal conductivity (W/cm-°C)	0.167-0.334		C177
Physical & Electrical Properties			
Specific gravity (g/cm^3)	1.28-1.32		D792
Water absorption (%weight increase)	2-7	after 24 hrs	D570
Dielectric strength (V/mil)			
1/8 " thick specimen	250-600		D149
Processing Properties			
Melting temperature (°C)	230	T_m, crystalline	

A4

Table A1. Physical characteristics of cellulose acetate (from [75]).

Characteristics	triacetate	secondary acetate
Density [g/cm^3]	1.27-1.29	1.28-1.32
Thermal stability [°C]	> 240	ca. 230
Tensile strength of fibers [kg/mm^2]	14-25	16-18
Tensile strength of foils [kg/mm^2]		
Longitudinal	12-14	8.5-10
Transverse	10-12	8.5-10
Refractive index of fibers relative to fiber axis		
Parallel	1.469	1.478
Perpendicular	1.472	1.473
Birefringence	-0.003	+0.005
Dielectric constant ε_r (50-60 Hz)	3.0-4.5	4.5-6.3
(10^6 Hz)		4.0-5.5
Dielectric loss factor tan δ (50-60 Hz)	0.01-0.02	0.03-0.04
(10^6 Hz)		0.04-0.06
Resistivity [Ω cm]	10^{13}-10^{15}	10^{11}-10^{13}
Heat capacity [J g^{-1} K^{-1}]	1.5	1.46-1.88
Thermal conductivity [J m^{-1} h^{-1} K^{-1}]		0.63-1.25

Acknowledgement

The support in literature search by Dr. A. Stein and Mrs. A. Sieg from Rhodia Acetow GmbH in Freiburg and Mrs. A. Peschel from the Institute of Physical Chemistry, TU Clausthal is gratefully acknowledged.